

Article (refereed) - postprint

Xu, Kai; Wu, Chuanhao; Zhang, Ce; Hu, Bill X.. 2021. **Uncertainty assessment of drought characteristics projections in humid subtropical basins in China based on multiple CMIP5 models and different index definitions.**

© 2020 Elsevier B.V.

This manuscript version is made available under the CC BY-NC-ND 4.0 license
<https://creativecommons.org/licenses/by-nc-nd/4.0/>



This version is available at <http://nora.nerc.ac.uk/id/eprint/530540/>

Copyright and other rights for material on this site are retained by the rights owners. Users should read the terms and conditions of use of this material at <https://nora.nerc.ac.uk/policies.html#access>.

This is an unedited manuscript accepted for publication, incorporating any revisions agreed during the peer review process. There may be differences between this and the publisher's version. You are advised to consult the publisher's version if you wish to cite from this article.

The definitive version was published in *Journal of Hydrology*, 600, 126502. <https://doi.org/10.1016/j.jhydrol.2021.126502>

The definitive version is available at <https://www.elsevier.com/>

Contact UKCEH NORA team at
noraceh@ceh.ac.uk

1 **Uncertainty assessment of drought characteristics projections in**
2 **humid subtropical basins in China based on multiple CMIP5**
3 **models and different index definitions**
4

5 Kai Xu^a, Chuanhao Wu^{a,b*}, Ce Zhang^{c,d}, Bill X. Hu^{a,b}

6 ^a *Institute of Groundwater and Earth Sciences, Jinan University, Guangzhou 510632,*
7 *China*

8 ^b *Green Development Institute of Zhaoqing, Zhaoqing, China*

9 ^c *Lancaster Environment Centre, Lancaster University, Lancaster LA1 4YQ, United*
10 *Kingdom*

11 ^d *UK Centre for Ecology & Hydrology, Library Avenue, Bailrigg, Lancaster LA1 4AP,*
12 *United Kingdom*

13

14

15

16

17

18

19

20

21

22 Author for correspondence

23 Chuanhao Wu (wuch0907@jnu.edu.cn)

24 Institute of Groundwater and Earth Sciences, Jinan University, Guangzhou 510632,

25 China.

26

27 **Abstract**

28 This study presents an assessment of projection and uncertainty of drought
29 characteristics (frequency D_F , drought area Da) using three drought indices (Palmer
30 Drought Severity Index, PDSI; Standardized Precipitation Index, SPI; Standardized
31 Precipitation Evapotranspiration Index, SPEI) in the humid subtropical Pearl River
32 basin in southern China during the period 2021-2050. The projection is based on 13
33 CMIP5 general circulation models (GCMs) under three Representative Concentration
34 Pathway scenarios (RCP2.6, RCP4.5 and RCP8.5). Specifically, the SPI is derived by
35 the precipitation simulations of 13 GCMs, whereas the PDSI and SPEI are computed
36 based on the simulations from the Variable Infiltration Capacity (VIC) model forced by
37 13 GCMs. The uncertainty of projected drought indices (PDSI, SPI and SPEI) due to
38 various GCMs and RCPs is quantified by the variance-based sensitivity analysis
39 approach. The results indicate that the sign and magnitude of the projected changes in
40 D_F and Da are highly dependent on the index definition at the regional scale, and the
41 SPI tends to underestimate the projected changes in D_F compared with PDSI and SPEI.
42 There is a large model spread in the projected D_F changes (especially for SPEI) under
43 all RCP scenarios, with larger model spread for more extreme drought events.
44 Uncertainty analysis shows that GCM contributes more than 90% of total uncertainty
45 in drought indices projections, while the RCP uncertainty is rather limited (< 10%)
46 compared with GCM. The GCM uncertainty is spatially unevenly distributed and shows
47 large variability at the interannual scale. This study highlights the sensitivity of drought
48 projections to the index definition as well as the large spatial-temporal variability of
49 general sources of uncertainty in drought projections.

50

51 **Key words:** Drought projection; Drought indices; uncertainty quantification; CMIP5;
52 RCPs

53

54 **1. Introduction**

55 Drought is a stochastic and recurring natural hazard that has devastating impacts on

56 economy, society, and ecosystem services around the world (Piao et al., 2010; Dai, 2011a;
57 Thornton et al., 2014; von Buttlar et al., 2018). The economic loss caused by drought
58 hazards is enormous, with an annual loss estimate of \$6~8 billion at a global scale
59 (Wilhite, 2000). The Intergovernmental Panel on Climate Change (IPCC)'s 4th and 5th
60 Assessment Report (AR4 and AR5) indicated that global surface mean temperature (T)
61 is likely to increase 0.3~4.8°C, accompanied by changes in spatial patterns and intensity
62 of precipitation (P) by the end of this century (IPCC, 2007; 2013). Global warming is
63 expected to exacerbate extreme events such as droughts, leading to significant changes
64 in area and intensity of drought all around the world (Dai, 2013; Cook et al., 2014;
65 Trenberth et al., 2014; Gudmundsson et al., 2017; Samaniego et al., 2018). Exploring
66 projected changes in drought intensity and frequency under various emission scenarios
67 can help prepare for future disaster prevention and mitigation, and support sustainable
68 development.

69

70 Drought is an abnormal phenomenon that can occur in short periods (days and weeks)
71 or long periods (months or longer), and can commonly be characterized by drought
72 monitoring indices. Typically, droughts are classified into four major types:
73 meteorological drought, hydrological drought, agricultural drought, and socioeconomic
74 drought (Heim, 2002; AMS, 2004; Hayes et al., 2011; Mishra and Singh, 2011).
75 Different types of drought have distinct spatiotemporal characteristics, and they vary at
76 different scales (Peters et al., 2006; Tallaksen et al., 2009). Meteorological drought is
77 identified by a prolonged lack of P as the main indicator, resulting in total soil moisture
78 (SM) deficits (i.e., agricultural drought) as well as the decrease of streamflow,
79 groundwater, reservoir and lake levels (i.e., hydrological drought). Such drought
80 hazards can also lead to severe consequence of drinking water scarcity, and negatively
81 impact crop yield and production, and result in economic loss. Socioeconomic
82 definitions of drought associate the supply and demand of certain economic good with
83 elements of meteorological, agricultural and hydrological drought (Wilhite and Glantz,
84 1985).

85

86 In the past decades, numerous indices have been proposed to quantify the drought and
87 wet conditions based on different hydroclimatic variables (e.g., T , P , evapotranspiration
88 ET , SM and runoff RO), of which the most commonly used is the Palmer Drought
89 Severity Index (PDSI; Palmer, 1965), the Rainfall Anomaly Index (RAI; van Rooy,
90 1965), the Crop Moisture Index (CMI; Palmer, 1968), the Soil Moisture Drought Index
91 (SMDI; Hollinger et al., 1993), the Surfacewater Supply Index (SWSI; Shafer and
92 Dezman, 1982), the Standardized Precipitation Index (SPI; Mckee et al., 1993, 1995),
93 the Standardized Runoff Index (SRI; Shukla and Wood, 2008), the Standardized
94 Precipitation Evapotranspiration Index (SPEI; Vicente-Serrano et al., 2010), and the
95 aridity index (AI; Huang et al., 2016). The use of different types of drought indices
96 often leads to different spatio-temporal variabilities of drought characteristics, even
97 though they are calculated using the inputs of hydroclimatic variables generated by the
98 same modeling system (Burke and Brown, 2008; Ukkola et al., 2018). For example,
99 PDSI and SPEI can measure the warming effect more explicitly through enhanced ET
100 than other drought indices based on P alone (e.g., SPI).

101

102 The General Circulation Models (GCMs), released by the Coupled Model
103 Intercomparison Project (CMIP), are the primary tools for estimating trends and
104 variability of future climate change (IPCC, 2007; 2013). Based on GCM simulations,
105 the influence of climate change on droughts have been investigated by numerous studies.
106 The majority of research indicated an increased drought risks over different regions
107 globally as the level of greenhouse gas (GHG) emission increases (e.g., Wang, 2005;
108 Sheffield and Wood, 2008; Li et al., 2012; Dai, 2011b, 2013; Cook et al., 2014; Wang
109 and Chen, 2014; Rhee and Cho, 2016; Wu et al., 2016; Zhao and Dai, 2017; Ruosteenoja
110 et al., 2018; Wang et al., 2018; Amnuaylojaroen et al., 2019; Rudd et al., 2019).
111 Although enormous efforts have been made to project how the drought risk would occur
112 as the result of GHG emission increase, few studies have assessed and quantified the
113 source of uncertainty in projecting future drought conditions. This uncertainty is due
114 mainly that drought is a complex process coupled with multiple meteorological factors
115 (e.g., P and ET), as well as various geomorphic and topographic characteristics of

116 specific regions. These key factors are described differently amongst GCMs, which
117 form the main source of uncertainty resulting in the lack of consistency between model
118 projections (Wang et al., 2018; Lee et al., 2019; Xu et al., 2019b; Wu et al., 2021).

119

120 This research focuses on Pearl River as the third longest River in China and composed
121 of West River, North River, East River, and Pearl River Delta. Pearl River is an
122 important source of fresh water for large cities in the Guangdong-Hong Kong-Macao
123 Greater Bay Area, such as Guangzhou, Zhuhai, Hong Kong and Macau (Zhang et al.,
124 2008). The Pearl River basin (PRB) is climatically humid with abundant P , but the
125 spatiotemporal distribution of P is uneven across the basin, with frequent extreme
126 weather events, such as floods and droughts. In recent years, the PRB has suffered from
127 droughts considerably with large severity and prolonged periods of water deficit,
128 presenting severe droughts events such as in 2004, 2005, 2010 and 2011 (Zhang et al.,
129 2012; Zhang et al., 2015; Wu et al., 2016; Chen et al., 2017; Xu et al., 2019a).

130

131 The temporal and spatial evolution of drought characteristics in the PRB has been
132 analyzed by several drought metrics (e.g. Zhang et al., 2009; Zhang et al., 2012; Fischer
133 et al., 2013; Niu et al., 2015; Xiao et al., 2016; Xu et al., 2019a). Recently, several
134 studies have projected changes in drought characteristics in the PRB under future
135 climate scenarios using CMIP5 models (Wu et al., 2016; Wang et al., 2018). For
136 example, Wang et al. (2018) predicted the spatiotemporal changes in future drought in
137 PRB using the PDSI and CMIP5 GCM simulations, and found that the severity of
138 drought would likely to be increased in the central and western regions of the PRB.
139 However, these studies were based solely on one drought index and a few models.
140 Previous research has reported that the sign and magnitude of projected drought is
141 highly dependent on the selection of drought index, region, and model ensemble (Burke
142 and Brown, 2008; Rhee and Cho, 2016; Ahmadalipour et al., 2017; Ukkola et al., 2018;
143 Lee et al., 2019). More importantly, general sources of uncertainty (e.g., GCMs and
144 RCP scenarios) in drought projection have not been explored in the PRB, and hence our
145 knowledge on uncertainties and their spatial and temporal variability in GCM-projected

146 drought remains limited at the basin scale.

147

148 To address this gap, our research presents a basin-scale assessment of future drought
149 characteristics projections in the PRB (including the West River and North River) by
150 using 13 CMIP5 GCMs, three RCP scenarios (RCP2.6, RCP4.5 and RCP8.5), and three
151 different drought indices (PDSI, SPI and SPEI). Specifically, an advanced hierarchical
152 sensitivity analysis is conducted to quantify the uncertainties in the projection of three
153 drought indices (PDSI, SPI and SPEI) due to three RCP scenarios and 13 GCMs at both
154 spatial and temporal scales. The objectives of this study are (1) to test the sensitivity of
155 projection of future drought characteristics with respects to index definition and various
156 model ensemble members and (2) to explore the spatio-temporal variability of
157 uncertainties of GCM and RCP, and rank the contribution of each uncertainty to the
158 projections of drought indices. In Section 2, detailed information on the observed and
159 modeling datasets for the study area, and the methods for bias correction, hydrological
160 modeling, drought indices and uncertainty estimation used in this study are provided.
161 Followed by the results and discussion presented in Sections 3 and 4, respectively.
162 Finally, the conclusions are drawn in Section 5.

163

164 **2. Study area and data source**

165 **2.1 Study area**

166 The Pearl River, located in southern China, is the third largest River in drainage basin
167 area in China (Fig.1). It consists of the West River, North River and East River as well
168 as the Rivers within the Pearl River delta. The water resources are unevenly distributed
169 spatially over the PRB and are mainly concentrated in the West River and North River
170 basins, account for approximately 93.7% of the total area of the PRB (Zhang et al.,
171 2013a). The PRB is characterized by tropical and subtropical climate zones, with mean
172 annual T ranging from 14 to 22 °C and mean annual P of approximately 1525 mm
173 (Zhang et al. 2012; Wu et al. 2013). The P over the PRB is mainly concentrated in the
174 flooding season between April and September, covering 80% of the total annual P

175 (Zhang et al. 2012). Due to climate warming, the hydrological cycle has become more
176 changeable over the PRB in recent years, resulting in an increased risk of extreme
177 flooding and drought (e.g., droughts in 2004, 2005, 2010, and 2011), influence
178 significantly on agriculture and ecological environment, and causing disastrous damage
179 to human lives and social economy.

180

181 **2.2 Data sources and processing**

182 **2.2.1 Meteorological and hydrological observations**

183 In this study, the observed data of meteorology and hydrology from 1971 to 2000 were
184 collected for analysis. The daily data of P , maximum/minimum T , and wind speed were
185 obtained from 57 meteorological stations (Fig.1) over the PRB as provided by the
186 National Meteorological Information Center (NMIC) of China Meteorological
187 Administration (<http://data.cma.cn>). For quality control of the observed data, we
188 checked any cases of maximum T less than minimum T or P values below 0 mm. The
189 daily record of the neighboring stations were also cross-compared, which helps to check
190 the correctness of values and any outliers. In addition, the homogeneity evaluation of
191 data was carried out and the test indicated that the meteorological data used were free
192 from severe errors (Wu et al., 2016). Daily runoff observations from the Gaoyao (1980-
193 2000) and Hengshi (1970-2000) hydrological stations, in the West River and North
194 River basins, were provided by the Hydrology Bureau of Guangdong Province, China.

195

196 **2.2.2 GCM simulations**

197 The downscaling results of the multimodel dataset of the 13 CMIP5 GCMs (Table 1)
198 were provided by the College of Global Change and Earth System Science, Beijing
199 Normal University. These 13 GCMs were chosen because they demonstrated well
200 performance in simulating the spatial and temporal variability of T and P over southern
201 China (Huang et al., 2013; Chen and Frauenfeld, 2014). The downscaling process of 13
202 GCMs is as follows: first, the monthly outputs of GCMs were interpolated to the sites
203 over the Pearl River basin by using the bilinear interpolation method, and corrected by

204 the observed data. Then the bias-corrected outputs of GCMs were weighted averaged
205 by the Bayesian model averaging method at the site scale, and were temporally
206 downscaled to multiple daily simulation samples (30 samples) using the stochastic
207 weather generation method according to the four categories (hot-wet, hot-dry, cold-wet,
208 and cold-dry) of the historical weather years. Finally, the daily simulations were
209 interpolated onto a common $0.25^\circ \times 0.25^\circ$ grid over the Pearl River basin using the
210 bilinear interpolation method. The detailed information on the statistical downscaling
211 process of the 13 GCMs can be found in Wu et al. (2014).

212

213 The downscaling simulations of these GCMs were used in this study, mainly because
214 of their good performance in reproducing daily variability of T and P in the Pearl river
215 basin (see Figures 4b and 5b in Wu et al., 2014). In addition, the multiple simulation
216 samples of the 13 GCMs can well represent the uncertainty range of GCMs. The daily
217 data for the baseline period 1971-2000 and the near future period 2021-2050 with three
218 different RCPs scenarios (i.e., RCP2.6, RCP4.5 and RCP8.5) are employed. For each
219 RCP scenario, a total of 30 simulation samples were collected to represent the
220 uncertainty range of GCMs.

221

222 **3. Methodology**

223 **3.1 Bias correction and adaptability assessment**

224 Many studies did not use climate model outputs directly for analyzing climate change
225 impact due to bias in GCM data (Lafon et al., 2013, Wu and Huang, 2016). In this
226 research, a “delta change” method was adopted to correct bias in T and P data of the
227 downscaling multi-model ensembles of 13 CMIP5 GCMs (Hay et al., 2000; Sperna
228 Weiland et al., 2010; Wu and Huang, 2016). For T (in units of $^\circ\text{C}$), an additive correction
229 was used:

$$230 \quad T_{cor,i,j} = T_{sim,i,j} + (\bar{T}_{obs,i,j} - \bar{T}_{sim,i,j}) \quad (1)$$

231 For P (in units of mm), a multiplicative correction was applied:

232
$$P_{cor,i,j} = P_{sim,i,j} \times \frac{\overline{P_{obs,i,j}}}{\overline{P_{sim,i,j}}} \quad (2)$$

233 where $(T_{cor,i,j})P_{cor,i,j}$ and $(T_{sim,i,j})P_{sim,i,j}$ are the bias-corrected and simulated i th
 234 daily $T(P)$, respectively, for the j th grid point. $\overline{T_{obs,i,j}}(\overline{P_{obs,i,j}})$ and $\overline{T_{sim,i,j}}(\overline{P_{sim,i,j}})$ are
 235 the 30-year averages of the observed and simulated i th daily $T(P)$, respectively, at
 236 the j th grid point for the baseline period 1971-2000.

237

238 3.2 VIC model

239 The VIC model is a macro-scale, semi-distributed hydrological model based on a grid-
 240 based land surface process scheme (Liang et al., 1994). It has the characteristics of ET
 241 calculation based on physical process, computation of water and energy balances
 242 simultaneously, and consideration of spatial heterogeneity in SM content of the grid
 243 (Liang et al., 1996). More detailed information about VIC model can be found at the
 244 University of Washington's website
 245 (<http://ftp.hydro.washington.edu/Lettenmaier/Models/VIC/>). As a typical land surface
 246 model, the VIC model has been successfully applied in the PRB for SM simulation (Niu
 247 et al., 2015) and the impact of climate change on hydrology by coupling with GCMs
 248 (e.g. Wu et al., 2014; Wu et al., 2015; Yan et al., 2015; Wang et al., 2018).

249

250 Here, the latest version VIC 5.0 model (<https://vic.readthedocs.io/en/master/>) was
 251 adopted to run at a spatial resolution of $0.25^\circ \times 0.25^\circ$ over the West and North River
 252 basins. The soil column of the model is divided vertically into three layers (top, middle
 253 and bottom), and the top and middle soil layers were considered for calculating the
 254 PDSI (Wang et al., 2018). The soil parameters were derived from the 1-km spatial
 255 resolution global soil classification and texture dataset provided by the FAO's
 256 Harmonized World Soil Database (HWSD) (FAO et al., 2009). The soil information
 257 was converted into soil hydraulic parameters based on Saxton and Rawls (2006). The
 258 land cover data were driven from the global 1-km land cover classification of the

259 University of Maryland (Hansen et al., 2000;
260 <https://www.geog.umd.edu/landcover/1km-map.html>). This dataset includes
261 vegetation-related parameters such as architectural resistance, leaf-area index, albedo,
262 minimum stomata resistance, and fraction of root depth of each soil layer. We assumed
263 that the land cover of the PRB would not change significantly in the future, and the land
264 cover data of 2000 was used for hydrological simulation over both baseline (1971-2000)
265 and the future period (2021-2050). The VIC model provides several daily output
266 variables for surface water fluxes calculation, including *ET*, *PET*, *SM* and runoff (*RO*).
267 The daily simulations of VIC model were aggregated into monthly time series to
268 compute the monthly water balance and drought indices (SPEI and PDSI).

269

270 **3.3 Drought indices**

271 **3.3.1 SPI and SPEI**

272 The SPI was originally developed to quantify the *P* deficit at multiple time-scales
273 (Mckee et al., 1993). Although the SPI considers only *P*, it has been widely used in
274 different meteorological, agricultural and hydrological applications thanks to its
275 simplicity in calculation and general applicability, as well as the consistency over space
276 and time (Hayes et al., 1999; Mishra et al., 2005; Zhang et al., 2009; Mishra and Singh,
277 2011; Huang et al., 2014; Zhu et al., 2016; Xu et al., 2019a). For SPI calculation, the
278 probability distribution is used initially to fit the long-term monthly *P*, and the
279 cumulative distribution function (CDF) is then turned into the normal distribution
280 through equal probabilities. The gamma distribution is used in this research to describe
281 the probability density function (PDF) of *P*:

$$282 \quad g(x) = \frac{1}{\beta^\alpha \tau(\alpha)} x^{\alpha-1} e^{-\frac{x}{\beta}} \quad (3)$$

283 where $\alpha > 0$ is a shape parameter, $\beta > 0$ denotes a scale parameter, and $\tau(\alpha)$ represents the
284 ordinary gamma function of α .

285

286 As an extension of the SPI, Vicente-Serrano et al. (2010) proposed the SPEI by

287 including both P and potential ET (PET) in identifying drought. Here, the PET was
 288 estimated by the FAO-56 Penman-Monteith (PM) method included in the VIC model
 289 (Allen et al., 1998). The SPEI was derived through the following steps: (1) the
 290 difference between P and PET for the i th month is calculated as: $D_i = P_i - PET_i$; (2) the
 291 D_i is aggregated at a certain (e.g., 3-month) timescale; and (3) the following log-logistic
 292 probability distribution $g(x)$ is used to fit the D_i to calculate SPEI:

$$293 \quad f(x) = \frac{\varphi}{\psi} \left(\frac{x-\gamma}{\psi} \right)^{\varphi-1} \left[1 + \left(\frac{x-\gamma}{\psi} \right)^{\varphi} \right]^{-2} \quad (4)$$

294 where φ , ψ , and γ are the scale, shape and origin parameters, respectively. The D is in
 295 the range of $\gamma < D < \infty$.

296

297 The SPI and SPEI can be used to quantify P deficit at multiple timescales (e.g., 1, 3, 6,
 298 12, 24 and 36 months). The short time scale SPI/SPEI (e.g., 1-month) reflects short-
 299 term dryness and wetness conditions and are sensitive to P short-term changes in
 300 general. Whereas, the long timescale SPI/SPEI (e.g., 24-month) reflects the long-term
 301 (small) variation of dryness and wetness (WMO, 2016). In this study, the 3-month scale
 302 is used to compute the SPI and SPEI (i.e., SPI3 and SPEI3) because it reflects seasonal
 303 variation of dryness and wetness conditions. The SPI is calculated based on the P from
 304 the GCMs outputs, and the SPEI is calculated based on the P from GCMs and PET
 305 simulated by the VIC model forced by the GCM outputs. The drought classifications
 306 based on the SPI and SPEI are shown in Table 2.

307

308 3.3.2 PDSI

309 The PDSI is based on the concept of climatically appropriate for existing conditions
 310 ($CAFEC$) proposed by Palmer (1965). It can be used to describe the degree of water
 311 deficit in a specific region less than the appropriate moisture content of the local climate.
 312 In this study, the P from the GCM outputs, and the PET , ET , SM (the top two soil layers)
 313 and RO simulated by the VIC model forced by the GCM outputs are used to estimate
 314 recharge to soils (R), water loss to soil layers (L), potential recharge (PR), potential
 315 runoff (PRO), and potential loss (PL) to derive $CAFEC$ at the monthly scale. Then the

316 PDSI is computed based on the difference between P and $CAFEC$. The $CAFEC$
 317 represents the amount of P required to keep a normal SM level for a given time, which
 318 is defined as:

$$319 \quad CAFEC = \alpha_i PET + \beta_i PR + \gamma_i PRO - \delta_i PL \quad (5)$$

320 where i indicates the calendar month of a year (from 1 to 12). α_i , β_i , γ_i and δ_i are
 321 climatological coefficients expressed as:

$$322 \quad \alpha_i = \frac{\overline{ET_i}}{\overline{PET_i}} \quad \beta_i = \frac{\overline{R_i}}{\overline{PR_i}} \quad \gamma_i = \frac{\overline{RO_i}}{\overline{PRO_i}} \quad \delta_i = \frac{\overline{L_i}}{\overline{PL_i}} \quad (6)$$

323 The difference between P and $CAFEC$ for a particular month is the moisture departure
 324 ($d = P - CAFEC$). The climatological standardization process aims to use d as a
 325 standardized drought index, considering local climate and drought duration, and the
 326 self-calibrating procedure (Wells et al., 2004):

$$327 \quad \begin{cases} Z = K_1 \times K_2 \times d_i \\ X_1 = qZ_1 \\ X_i = pX_{i-1} + qZ_i \end{cases} \quad (7)$$

328 where Z is the moisture anomaly index for the i th month; K_1 denotes the temporal
 329 correction weight; K_2 represents the spatial correction weight; p and q are duration
 330 factors; and X_{i-1} is the PDSI for the previous month. For more information on the
 331 calculation of K_1 , K_2 , p and q , please refer to Wells et al. (2004). Table 2 shows the
 332 classification of drought in accordance to the PDSI definition.

333

334 3.3.3 Drought area and frequency

335 Based on the classification definition of drought (Table 2), a threshold value of -1 (-0.5)
 336 for PDSI (SPI/SPEI) is used to identify the occurrence of drought. Drought area is
 337 defined as:

$$338 \quad D_a = \frac{\sum_{i=1}^n d_a}{n_a} \times 100 \quad (8)$$

339 where D_a is the percentage of drought area (%), d_a is the number of grid points with
 340 $PDSI \leq -1$ ($SPI/SPEI \leq -0.5$), and n_a is total number of grid points.

341
$$D_F = \frac{n_m}{N_m} \times 100 \quad (9)$$

342 where D_F is the drought frequency (%), n_m and N_m are the number of drought months
 343 and the total number of months, respectively.

344

345 **3.4 Variance-based sensitivity analysis framework**

346 In this study, the variance-based two-layer sensitivity analysis framework was used to
 347 quantify the uncertainty of GCMs and RCP scenarios in the projection of future drought
 348 indices (Dai et al., 2017; Xu et al., 2019b). In this framework, the model with a form of

349 $\Delta = f(\theta) = f(\theta_1, \dots, \theta_k)$ is a set of uncertain model inputs, with total variance ($V(\Delta)$)

350 being decomposed as:

351
$$V(\Delta) = V_{\theta_i}(E_{\theta_{-i}}(\Delta | \theta_i)) + E_{\theta_i}(V_{\theta_{-i}}(\Delta | \theta_i)) \quad (10)$$

352 where Δ is the objective function of the model output and $\theta = \{\theta_1, \dots, \theta_k\}$.

353 $V_{\theta_i}(E_{\theta_{-i}}(\Delta | \theta_i))$ is the partial variance contributed by θ_i , while $E_{\theta_i}(V_{\theta_{-i}}(\Delta | \theta_i))$

354 represents the partial variance caused by model inputs apart from θ_i and interactions
 355 amongst all inputs (Dai and Ye, 2015; Dai et al., 2017).

356

357 Based on Eq. (10), the total variance ($V(\Delta)$) is decomposed as:

358
$$\begin{aligned} V(\Delta) &= E_{\mathbf{R}}V_{\mathbf{S}|\mathbf{R}}(\Delta | \mathbf{R}) + V_{\mathbf{R}}E_{\mathbf{S}|\mathbf{R}}(\Delta | \mathbf{R}) \\ &= V(\mathbf{S}) + V(\mathbf{R}) \end{aligned} \quad (11)$$

359 where \mathbf{R} is the set of multiple RCP scenarios, and \mathbf{S} is the set of multiple GCMs. The
 360 subscript $\mathbf{S}|\mathbf{R}$ indicates the change of GCMs under particular RCP scenario. The terms
 361 in Eq. (11) refer to variances from RCP scenarios and GCMs uncertainty, respectively.

362 The sensitivity of RCPs (S_R) and GCMs (S_S) can then be determined as follows:

363
$$\begin{aligned} S_R &= \frac{V_{\mathbf{R}}E_{\mathbf{S}|\mathbf{R}}(\Delta | \mathbf{S}, \mathbf{R})}{V(\Delta)} = \frac{V(\mathbf{R})}{V(\Delta)} \\ S_S &= \frac{E_{\mathbf{R}}V_{\mathbf{S}|\mathbf{R}}(\Delta | \mathbf{S}, \mathbf{R})}{V(\Delta)} = \frac{V(\mathbf{S})}{V(\Delta)} \end{aligned} \quad (12)$$

364 For each drought index (PDSI, SPI3 and SPEI3), the mean and variance of outputs with
 365 respects to uncertainty from GCMs under certain RCP scenario are calculated, and the
 366 mean and variance of RCP scenarios are quantified. Assume that there are k alternative
 367 RCP scenarios and n plausible GCMs for each RCP scenario, the uncertainty of GCMs
 368 is estimated as:

$$\begin{aligned}
 V(\mathbf{S}) &= E_{\mathbf{R}} V_{\mathbf{S}|\mathbf{R}}(\Delta | \mathbf{S}, \mathbf{R}) \\
 369 \quad &= \sum_k \left(\frac{1}{n} \sum_{i=1}^n \Delta^2(S_i | R_k) - \left(\frac{1}{n} \sum_{i=1}^n \Delta(S_i | R_k) \right)^2 \right) P(R_k) \quad (13)
 \end{aligned}$$

370 where $P(R_k)$ is the weight of RCP scenario, subject to $\sum_k P(R_k) = 1$, and the
 371 uncertainty of RCP scenarios is deduced as:

$$\begin{aligned}
 V(\mathbf{R}) &= V_{\mathbf{R}} E_{\mathbf{S}|\mathbf{R}}(\Delta | \mathbf{R}) \\
 372 \quad &= E_{\mathbf{R}} \left(E_{\mathbf{S}|\mathbf{R}}(\Delta | \mathbf{R}) \right)^2 - \left(E_{\mathbf{R}} E_{\mathbf{S}|\mathbf{R}}(\Delta | \mathbf{R}) \right)^2 \quad (14) \\
 &= \sum_k P(R_k) \left(\frac{1}{n} \sum_{i=1}^n \Delta(S_i | R_k) \right)^2 - \left(\sum_k \left(\frac{1}{n} \sum_{i=1}^n \Delta(S_i | R_k) \right) P(R_k) \right)^2
 \end{aligned}$$

373

374 4. Results

375 4.1 Evaluation of GCM and VIC simulations

376 Fig. 2 shows the comparison between the observed and bias-corrected monthly average
 377 T and P of 30 simulation samples of 13-GCM ensembles in the West River (Fig. 2a, 2c)
 378 and North River (Fig. 2b, 2d) basins for the baseline period 1971-2000. As shown in
 379 Fig. 2, the majority of model simulations reproduce the intra-annual variability of T
 380 reasonably well (despite a bit underestimation in a few months). Compared with T ,
 381 greater uncertainty range is identified in the simulations of P , especially in the flood
 382 season (May-August). Moreover, larger uncertainty range is found in the North River
 383 basin compared to the West River basin. Overall, the bias-corrected model simulations
 384 can simulate the intra-annual variability of P for the two basins, particularly for the dry
 385 season (October-March).

386

387 Fig. 3 demonstrates the comparison of simulated and observed daily discharges at the

388 Gaoyao and Hengshi stations for the calibration and validation periods. The daily Nash-
389 Sutcliffe efficiency coefficient (NSE) at the Gaoyao and Hengshi stations are 0.85 and
390 0.9 (0.89 and 0.9) in the calibration (validation) period, respectively, and the relative
391 errors (Res) are 7.25% and 2.95% (0.21% and 0.42%), respectively, in the calibration
392 (validation) period. Overall, the VIC model can reproduce the low discharge accurately
393 during dry season and the flood peak during flooding season, and the occurrence time
394 is generally consistent between the observed and simulated ones, indicating that the
395 VIC model is applicable for subsequent GCM-projections of drought.

396

397 Fig. 4 shows the comparison of the simulated PDSI, SPI3 and SPEI3 with the observed
398 ones in the West and North River basins during the baseline period 1971-2000. As
399 witnessed in Fig. 4, the model simulations tend to underestimate the variability of PDSI,
400 SPI3 and SPEI3, and fail to capture some extreme wet and dry events in wet and dry
401 years, particularly in the West River basin. Compared with PDSI, the temporal
402 variability of SPI and SPEI tends to be large for both basins, bringing challenges for the
403 model to simulate the dryness/wetness conditions characterized by SPI and SPEI.
404 Overall, the three drought indices are simulated more accurately in the North River
405 basin than West River basin.

406

407 **4.2 Sensitivity of projected D_a changes to index definition, GCM** 408 **ensemble and RCP**

409 This section focuses on the sensitivity analysis of projected drought area changes to
410 index definition, GCM ensemble and RCP scenario. Fig. 5 reveals the temporal
411 evolutions (2021-2050) of the projected changes in D_a indicated by the PDSI (≤ -1),
412 SPI3 (≤ -0.5) and SPEI3 (≤ -0.5) for the future period 2021-2050 (relative to the baseline
413 period) in the two basins under three RCP scenarios. Clearly, there are obvious
414 differences in projected D_a changes between different indices. However, compared with
415 PDSI, SPI and SPEI demonstrate more similar and larger temporal variability of the
416 projected D_a changes for both basins. Large GCM spread (uncertainty range) is found

417 in projected D_a changes, especially in the North River basin, which is significantly
418 larger than that of drought indices and RCPs. In contrast, there are relatively small
419 differences in projected D_a changes under three RCP scenarios compared with GCMs
420 and drought indices.

421

422 **4.3 Sensitivity of projected D_F changes to index definition, GCM** 423 **ensemble and RCP**

424 This section focuses on the sensitivity analysis of the projected D_F to index definition,
425 GCM ensemble and RCP scenario. The projected D_F changes indicated by the PDSI,
426 SPI3 and SPEI3 with extreme, severe, moderate and mild drought events for the West
427 and North River basins during the future period 2021-2050 under three RCP scenarios
428 were calculated (relative to the baseline period 1971-2000).

429

430 Fig.6 shows the uncertainty range (GCM spread) of the projected D_F changes (%)
431 indicated by three drought indices under three RCP scenarios. From the figure, clearly
432 there is a large GCM spread in the projected D_F changes (especially for that indicated
433 by SPEI) under all RCP scenarios, with the larger GCM spread in the North River basin
434 than West River basin. In contrast, the RCP discrepancy in the projected D_F changes is
435 generally smaller compared with GCM. In terms of drought events, larger GCM
436 uncertainty range is found for the projected changes in extreme drought than other
437 drought events. There are also large discrepancies in the sign and magnitude of the
438 projected D_F changes amongst three drought indices (especially between SPI and
439 PDSI/SPEI). The SPI tends to underestimate the projected changes in D_F compared
440 with PDSI and SPEI in the West River basin.

441

442 Fig.6a also reveals the increased D_F indicated by the PDSI (SPEI3) is projected for all
443 drought events (extreme, severe, moderate and mild) in the West River basin, especially
444 for extreme drought, with the mean increases up to 15% (13.7%), 13% (12.3%) and
445 13.3% (13%) under RCP2.6, RCP4.5 and RCP8.5, respectively. In comparison, the

446 SPI3 detects an increase in extreme drought, with average increase of 10.4%, 10% and
447 9.1% under RCP2.6, RCP4.5 and RCP8.5, respectively, and a decrease in severe
448 (moderate) drought, with average decrease of -5.3% (-12%), -5.3% (-12%) and -4.9%
449 (-11.6%) under RCP2.6, RCP4.5 and RCP8.5, respectively.

450

451 For the North River basin (Fig.6b), the D_F of extreme and mild droughts indicated by
452 three drought indices (PDSI, SPI3 and SPEI3) shows an overall increase under three
453 RCP scenarios. Particularly, SPI3 detects large mean increase in extreme drought (up
454 to 10.1%, and 9.1% and 11.7% under RCP2.6, RCP4.5 and RCP8.5, respectively),
455 whereas SPEI3 detects large mean increase in mild drought (up to 18.3%, and 18.6%
456 and 17.9% under RCP2.6, RCP4.5 and RCP8.5, respectively). In contrast, the D_F of
457 severe drought indicated by three indices is projected to decrease under all 3 RCP
458 scenarios, and SPEI3 shows large mean decrease compared with other indices (up to -
459 11.4%, -12.3% and -10.7% under RCP2.6, RCP4.5 and RCP8.5, respectively). For
460 moderate drought, the projected increases in D_F are indicated by PDSI (SPEI3), with
461 mean increase of 8.4% (1.6%), 8.7% (2.0%) and 8.3% (1.5%) under RCP2.6, RCP4.5
462 and RCP8.5, respectively.

463

464 **4.4 Spatial distributions of the projected D_F changes**

465 The spatial distribution of the multi-GCM ensemble mean changes in D_F (indicated by
466 the PDSI, SPI3 and SPEI3) with extreme, severe, moderate and mild drought events for
467 the future period 2021-2050 (relative to the baseline period 1971-2000) under three
468 RCP scenarios are displayed in Figs. 7 and 8 for the West River and North River basins,
469 respectively. Figs. 7 and 8 highlight the sign and magnitude of D_F changes, which are
470 dependent on the index definition, particularly for the North River basin. For a certain
471 drought index, there are significant spatial variation in model projection for both basins.

472

473 For the West River basin (Figs.7a~c), there are large spatial difference in the projected
474 D_F changes between SPI and PDSI (SPEI), while similar spatial pattern can be found

475 between PDSI and SPEI3. The projected D_F changes in extreme drought indicated by
476 the PDSI and SPEI3 tend to be more significant than other drought events. The largest
477 D_F changes in extreme drought indicated by the PDSI (15.9%) and SPEI3 (16.4%) are
478 concentrated in the downstream reaches of the West basin, while the decreases are
479 projected mainly in the upstream areas (up to -23.7% and -15.7%, respectively). For
480 SPI3, the projected D_F changes are unevenly distributed in the West River basin, with
481 the largest increase of 9.5% in extreme D_F under RCP8.5 (Fig. 7b). In contrast, the D_F
482 of moderate and mild droughts is projected to decrease in the majority of the West River
483 basin, particularly under RCP4.5 and RCP8.5 (up to -16.7%).

484

485 For the North River basin (Figs.8a~c), the projected D_F changes indicated by three
486 drought indices are unevenly distributed at the spatial scale. For PDSI, the D_F of
487 moderate and mild droughts shows larger increase compared with other drought events
488 in major North River basin under three RCP scenarios (Fig. 8a). The D_F of mild drought
489 is increased by 11.3% under RCP2.6, while that of extreme and severe droughts is
490 decreased, especially for severe drought (up to -7.8%). For SPI3, the D_F of extreme
491 drought is projected to increase in the majority of the North River basin under RCP2.6
492 and RCP4.5 (up to 8.2%), and decrease in the northern parts of the North River basin
493 under RCP8.5 (up to -8.2%). For SPEI3, the projected D_F changes are spatially
494 heterogeneous in the North River basin, with the largest increase of 11.8% in D_F of
495 extreme drought under RCP8.5 (Fig. 8c). In contrast, the D_F of severe drought is
496 projected to decrease in most of the North River basin, especially in the northern regions
497 under RCP2.6 and RCP4.5 (up to -16%).

498

499 **4.5 Sensitivity indices for the uncertainty contributions to the drought** 500 **indices projections**

501 The sensitivity indices for the uncertainty contribution of GCM and RCP to the
502 projection of three drought indices (PDSI, SPI and SPEI) were calculated at both spatial
503 (basin) and temporal (interannual) scales using the variance-based sensitivity analysis

504 approach. Fig.9 shows the temporal evolution (2021-2050) of uncertainty contribution
505 (i.e., sensitivity indices) of GCM and RCP to three drought indices (PDSI, SPI and SPEI)
506 projections during the period 2021-2050. From the Figure, GCM plays a dominant role
507 (> 90%) in the projection uncertainty of three drought indices over the entire period for
508 both basins, whereas the uncertainty of RCP is relatively limited compared with GCM.
509 The GCM (RCP) uncertainty tends to be larger (smaller) in the West River basin than
510 the North River basin, while the interannual variability of GCM (RCP) uncertainty is
511 larger in the North River basin than in the West River basin. Overall, the GCM (RCP)
512 uncertainty presents similar pattern amongst three drought indices, but tends to be
513 smaller (larger) in SPI3 than PDSI and SPEI3 projections for both basins.

514

515 Fig.10 demonstrates the spatial distribution of GCMs' uncertainty contribution to the
516 projection of PDSI, SPI3 and SPEI3 in the two basins during future three decades (i.e.,
517 2030, 2040 and 2050). As shown in Fig.10, GCM is the leading uncertainty source (>
518 90%) for the projection of three drought indices for both basins. The uncertainty of
519 GCM is unevenly distributed but with similar spatial patterns among three drought
520 indices in the West River basin (Fig.10a). In addition, the uncertainty of GCM tends to
521 increase (decrease) in the eastern (southwest) regions from 2030 to 2050, while in the
522 southern regions it decreases first and then increases. For the North River basin
523 (Fig.10b), the uncertainty of GCM is unevenly distributed and shows large spatial
524 discrepancies among three drought indices. Overall, the uncertainty of GCM
525 (particularly for the projection of PDSI and SPEI3) tends to decrease in the majority of
526 the North River basin from 2030 to 2050, especially in northeast and southern regions
527 (Fig. 10b).

528

529 Fig.11 reveals the overall uncertainty contributions of GCM and RCP to the projection
530 of three drought indices (PDSI, SPI3, and SPEI3) for the two basins. Overall, GCM
531 contributes more than 96% of total uncertainty to the PDSI projection for both basins,
532 while for the projection of SPI3 and SPEI3, the uncertainty contribution of GCM takes
533 over 95% for both basins. Compared with GCM, the uncertainty of RCP is rather

534 limited and can be omitted in the future period (2021-2050) for both basins.

535

536 **5. Discussion**

537 In this research, we present an assessment of projection and uncertainty of D_F and D_a
538 in the Pearl River basin during the period 2021-2050 based on downscaling simulations
539 (a total of 90 samples) of 13 CMIP5 GCMs under three RCP scenarios. Three different
540 drought indices (i.e., PDSI, SPI3 and SPEI3) are employed to explore the spatio-
541 temporal changes in D_F and D_a with different (extreme, severe, moderate and mild)
542 drought events. The uncertainty in the projection of three drought indices derived from
543 GCMs and RCPs is quantified using variance-based sensitivity analysis approach.

544

545 The results show that the sign and magnitude of the projected changes in drought
546 characteristics (e.g., D_F and D_a) are highly dependent on the index definition at both
547 spatial and temporal scales, generally consistent with the findings from previous studies
548 (e.g., Burke and Brown, 2008; Mishra and Singh, 2010; Touma et al., 2015; Lee et al.,
549 2019; Yang et al., 2019). This suggests that any single index may suffer from limitations
550 in considering the different aspects of droughts comprehensively. In particular, the SPI
551 tends to underestimate the projected changes in D_F in both basins compared with PDSI
552 and SPEI, which might be due to that the SPI considers P deficit alone without taking
553 into account the impact of ET in the context of climate warming (Jeong et al., 2014;
554 Rhee and Cho, 2016; Yoo et al., 2016; Ahmadalipour et al., 2017; Huang et al., 2018;
555 Lee et al., 2019; Haile et al., 2020; Wu et al., 2020).

556

557 The results also highlight a large discrepancy in the projected D_F and D_a changes
558 amongst different GCM ensembles (Figs. 4-6), and larger model spread is found in the
559 projected D_F and D_a changes of extreme drought than other drought events (Fig.6). This
560 is in consistency with previous studies showing a large uncertainty among GCMs when
561 projecting drought events in 21st century using CMIP3 and CMIP5 ensemble (Sheffield
562 and Wood, 2008; Dai, 2013; Orlowsky and Seneviratne, 2013). The uncertainty analysis

563 suggests that the GCM uncertainty, as expected, plays an important role (contribution >
564 90%) in the projections of drought indices in both basins, while the uncertainty of RCP
565 is generally limited compared with GCM (Figs. 9 and 11). This is supported by Figs. 5
566 and 6, showing that there are larger discrepancies in projected D_a and D_F among GCM
567 ensembles than RCPs. Such finding is also generally consistent with the previous
568 studies on the projection of meteorological droughts (Wu et al., 2021), extreme
569 temperatures (Wilby and Harris 2006; Woldemeskel et al., 2016; Xu et al., 2019c),
570 precipitation (Zhou et al, 2014; Woldemeskel et al., 2016; Hosseinzadehtalaei et al,
571 2017; Zarekarizi et al., 2018; Xu et al., 2019b; Kim et al., 2020), and floods (Graham et
572 al., 2007; Kay et al., 2009; Jung et al., 2011; Addor et al, 2014; Giuntoli et al., 2015;
573 Vetter et al., 2017). All these literatures indicated that the uncertainty caused by GCM
574 is larger than that of RCP.

575

576 This study also highlights a large spatio-temporal variability of uncertainty in the
577 regional projection of drought characteristics. At the spatial scale, the uncertainty of
578 GCM is unevenly distributed and show similar spatial patterns amongst three drought
579 indices in the West River basin, while in the North River basin the uncertainty of GCM
580 shows large spatial discrepancies amongst three drought indices (Fig.10). At the
581 interannual scale, the uncertainty of GCM shows a large variability, and the variability
582 tends to be larger in the North River basin than in the West River basin (Fig.9). This is
583 generally consistent with the previous studies (Xu et al., 2019b; Wu et al., 2021), which
584 indicated that the uncertainty of GCM and RCP in drought prediction has large temporal
585 and spatial variations at the regional scale. Spatially, GCM has relatively larger
586 uncertainty in the Southern Hemisphere than the Northern Hemisphere, whereas RCP
587 has relatively larger uncertainty in the Northern Hemisphere than the Southern
588 Hemisphere (Wu et al., 2021). At the temporal scale, the GCM uncertainty shows
589 overall decreasing trends with time (Xu et al., 2019b; Wu et al., 2021). In contrast, the
590 RCP uncertainty is expected to increase over time until the end of this century, but
591 remains less than that of GCM at the regional (Xu et al., 2019b) and global (Wu et al.,
592 2021) scales. The spatio-temporal variability of the uncertainties in GCM-based

593 drought projection, might be due to the results of disagreement on the magnitude of
594 warming, as well as the magnitude and sign of P changes at the regional scale
595 (Trenberth et al., 2014).

596

597 Within this study, we did not consider some other potential sources of uncertainty that
598 arise not only from the methods but also from the simulations themselves. First,
599 although the bias-corrected method shows significant improvement in the simulations
600 of T and P , there are still relatively large errors (especially for P) in few months (see
601 Fig. 2), which may lead to potential uncertainty. Particularly, the GCM simulations fail
602 to capture some extreme events in wet/dry years, particularly in the West River basin
603 (Fig. 4). This means that the bias-corrected method may reduce the variability range of
604 the GCM simulations, leading to an underestimation of GCM uncertainty in the
605 projections of drought indices (SPI, PDSI, SPEI) during extreme wet and dry years.
606 This is supported by Wu et al. (2021), which indicated that the bias-corrected method
607 can be an important uncertainty source in explaining the model difference in the
608 projection of meteorological droughts. Second, the definitions of D_F and D_a are based
609 only on the threshold of (-1 for PDSI and -0.5 for SPI and SPEI) of drought indices,
610 without quantifying the drought events statistically. The choice of methods to define
611 drought characteristics can also lead to model discrepancies in drought projection (Mo,
612 2008; Sheffield and Wood, 2008; Dai, 2011b). In addition, we only consider one
613 hydrological model (VIC) in the hydrological simulations. Hydrological models
614 themselves may be biased due to inadequacies in the modeled physical processes and
615 parameterizations and because of processes that are not include in the modeling, the
616 structure of hydrological model can be an important source of uncertainty in climate
617 change assessment (Graham et al., 2007; Kay et al., 2009; Addor et al., 2014; Eisner et
618 al., 2017; Su et al., 2017; Vetter et al., 2017; Ju et al., 2021). The PDSI and SPEI were
619 partly calculated based on hydrological simulations. This means that the uncertainty of
620 hydrological model is included in the uncertainty of GCM and RCP, which may lead to
621 the overestimation of the uncertainty of GCM and RCP in the projections of PDSI and
622 SPEI. In future research, it would be interesting to explore more sources of uncertainty

623 (e.g., hydrological model, bias-corrected method, and the definition of drought) with
624 the consideration of multiple-model ensembles, which are essential for assessing
625 drought projection reliably in response to climate warming at both regional and basin
626 scales.

627

628 **6. Conclusions**

629 This research assesses the projection and uncertainty of drought characteristics (D_F and
630 D_a) in the Pearl River basin during the period 2021-2050 using three different drought
631 indices (PDSI, SPI and SPEI) based on 13 CMIP5 GCMs under three RCP scenarios.
632 The SPI is calculated based on the P simulations of 13 GCMs, while the PDSI and SPEI
633 are computed based on the simulations of the VIC model forced by 13 GCMs. The
634 uncertainty of projected drought indices (PDSI, SPI and SPEI) due to various GCMs
635 and RCPs is quantified by the variance-based sensitivity analysis approach.

636

637 The results show that there are large discrepancies in the sign and magnitude of D_F and
638 D_a changes amongst three drought indices, and the SPI tends to underestimate the
639 projected changes in D_F in both basins compared with PDSI and SPEI. In terms of a
640 particular drought index, there are significant spatial variation in the model projection
641 of D_F . There is also a large model spread in the projected D_F and D_a changes among
642 different GCM ensembles, and larger model spread is found in the projected extreme
643 drought than other drought events. Overall, the D_F of extreme drought is projected to
644 increase in the future period (2021-2050) in both basins, especially for the North River
645 basin.

646

647 The uncertainty analysis results show that GCM is the dominant uncertainty
648 (contribution > 90%) in the projections of three drought indices, while the uncertainty
649 of RCP is relatively limited compared with GCM. The uncertainty of GCM and RCP
650 shows a large interannual variability during the future period, with larger variability in
651 the North River basin than Wet River basin. At the spatial scale, the uncertainty of GCM

652 is unevenly distributed and show similar spatial patterns among three drought indices
653 in the West River basin, while the uncertainty of GCM in the North River basin shows
654 large spatial discrepancies amongst three drought indices. By the end of 2050, the
655 uncertainty of GCM tends to increase in the Eastern regions of the Wet River basin and
656 decrease in the Northeast and Southern regions of the North River basin. This study
657 highlights the sensitivity of drought projection to the index definition as well as the
658 large spatial-temporal variability of general uncertainty sources in drought projections.

659

660 **Acknowledgements**

661 This research was supported by funding from the 2019 International Program of
662 Guangdong Provincial Outstanding Yong Researcher, the China Postdoctoral Science
663 Foundation (Grant No. 2020M673073), the National Natural Science Foundation of
664 China (Grant No. 51909106, 51879108, 51709127), the Natural Science Foundation of
665 Guangdong Province, China (Grant No. 2020A1515011038, 2018A030310653), the
666 high-level talent project for the “Pearl River Talent Plan” of Guangdong Province
667 (Grant No. 2017GC010397), and the Youth Innovative Talents Project for Guangdong
668 Colleges and Universities (Grant No. 2017KQNCX010).

669

670 **References**

- 671 Addor N., Rössler O., Köplin K., Huss M., Weingartner R., Seibert J., 2014. Robust changes and
672 sources of uncertainty in the projected hydrological regimes of Swiss catchments. *Water*
673 *Resour. Res.*, 50, 7541–7562. <https://doi.org/10.1002/2014WR015549>.
- 674 Ahmadalipour A., Moradkhani H., Demirel M.C., 2017. A comparative assessment of projected
675 meteorological and hydrological droughts: Elucidating the role of temperature. *J. Hydrol.*, 553,
676 785–797. <https://doi.org/10.1016/j.jhydrol.2017.08.047>.
- 677 Allen R.G., Pereira L.S., Raes D. & Smith M., 1998. Crop Evapotranspiration-Guidelines for
678 computing crop water requirements. Food and Agricultural Organization of the United Nations
679 Irrigation and Drainage Paper, 56 300 (8): D05109.
- 680 American Meteorological Society (AMS), 2004. Statement on Meteorological Drought. *Bull. Am.*
681 *Meteorol. Soc.*, 85, 771–773.
682 https://www.ametsoc.org/POLICY/2013drought_amsstatement.html.
- 683 Amnuaylojaroen T., Chanvichit P., 2019. Projection of near-future climate change and agricultural
684 drought in Mainland Southeast Asia under RCP8.5. *Clim. Chang.*, 155(2), 175–193.

685 <https://doi.org/10.1007/s10584-019-02442-5>.

686 Burke E.J., Brown S.J., 2008. Evaluating uncertainties in the projection of future drought. *J.*
687 *Hydrometeorol.*, 9(2), 292–299. <https://doi.org/10.1175/2007JHM929.1>.

688 Cook B.I., Smerdon J.E., Seager R., Coats S., 2014. Global warming and 21st century drying. *Clim.*
689 *Dyn.*, 43(9-10), 2607–2627. <https://doi.org/10.1007/s00382-014-2075-y>.

690 Chen J., Brissette F.P. & Leconte R., 2011. Uncertainty of downscaling method in quantifying the
691 impact of climate change on hydrology. *J. Hydrol.*, 401(3-4), 190–202.
692 <https://doi.org/10.1016/j.jhydrol.2011.02.020>.

693 Chen L., Frauenfeld O.W., 2014. Surface air temperature changes over the twentieth and twenty-
694 First centuries in China simulated by 20 CMIP5 models. *J. Clim.*, 27 (11), 3920–3937.
695 <https://doi.org/10.1175/JCLI-D-13-00465.1>.

696 Chen Y.D., Zhang Q., Xiao M., Singh V.P., 2017. Transition probability behaviors of drought events
697 in the Pearl River basin, China. *Stoch. Environ. Res. Risk Assess.*, 31(1), 159–170.
698 <https://doi.org/10.1007/s00477-015-1178-2>.

699 Dai A.G., 2011a. Characteristics and trends in various forms of the Palmer Drought Severity Index
700 during 1900-2008. *J. Geophys. Res.*, 116(D12), 1248–1256.
701 <https://doi.org/10.1029/2010JD015541>.

702 Dai A.G., 2011b. Drought under global warming: A review. *Wiley Interdiscip. Rev.: Clim. Change*,
703 3, 52–58. <https://doi.org/10.1002/wcc.81>; Corrigendum, 3, 167,
704 <https://doi.org/10.1002/wcc.190>.

705 Dai A.G., 2013. Increasing drought under global warming in observations and models. *Nat. Clim.*
706 *Change.*, 3(2), 52–58. <https://doi.org/10.1038/NCLIMATE1633>.

707 Dai H., Ye M., 2015. Variance-based global sensitivity analysis for multiple scenarios and models
708 with implementation using sparse grid collocation. *J. Hydrol.*, 528, 286–300.
709 <https://doi.org/10.1016/j.jhydrol.2015.06034>.

710 Dai H., Ye M., Walker A.P., Chen X.Y., 2017. A new process sensitivity index to identify important
711 system processes under process model and parametric uncertainty. *Water Resour. Res.*, 53,
712 3476–3490. <https://doi.org/10.1002/2016WR019715>.

713 Eisner S., Flörke M., Chamorro A., et al. 2017. An ensemble analysis of climate change impacts on
714 streamflow seasonality across 11 large river basins. *Clim. Change*, 141(3), 401–417.
715 <https://doi.org/10.1007/s10584-016-1844-5>.

716 FAO, IIASA, ISRIC, ISSCAS, 2009. Harmonized World Soil Database Version 1.1.

717 Fischer T., Gemmer M., Liu L.L., Su B.D., 2011. Temperature and precipitation trends and
718 dryness/wetness pattern in the Zhujiang River Basin, South China, 1961-2007. *Quatern. Int.*,
719 244(2), 138–148. <https://doi.org/10.1016/j.quaint.2010.08.010>.

720 Fischer T., Gemmer M., Su B., Scholten T., 2013. Hydrological long-term dry and wet periods in
721 the Xijiang River basin, South China. *Hydrol. Earth Syst. Sci.*, 17 (1), 135–148.
722 <https://doi.org/10.5194/hess-17-135-2013>.

723 Fowler H.J., Blenkinsop S., Tebaldi C., 2007. Linking climate change modelling to impacts studies:
724 recent advances in downscaling techniques for hydrological modelling. *Int. J. Climatol.*, 27,
725 1547–1578. <https://doi.org/10.1002/joc.1556>.

726 Giuntoli I., Vidal J.P., Prudhomme C., and Hannah D.M., 2015. Future hydrological extremes: the
727 uncertainty from multiple global climate and global hydrological models. *Earth Syst. Dynam.*,
728 6, 267–285. <https://doi.org/10.5194/esd-6-267-2015>.

729 Graham L.P., Hagemann S., Jaun S. and Beniston M., 2007. On Interpreting Hydrological Change
730 From Regional Climate Models. *Clim. Change*, 81, 97–122. [https://doi.org/10.1007/s10584-](https://doi.org/10.1007/s10584-006-9217-0)
731 [006-9217-0](https://doi.org/10.1007/s10584-006-9217-0).

732 Gudmundsson L., Seneviratne S.I., and Zhang X., 2017. Anthropogenic climate change detected in
733 European renewable freshwater resources. *Nat. Clim. Change*, 7(11), 813–816.
734 <https://doi.org/10.1038/nclimate3416>.

735 Haile G.G., Tang Q., Hosseini-Moghari S.-M., Liu X., Gebremicael T.G., Leng G., Kebede A., Xu
736 X., and Yun X., 2020. Projected impacts of climate change on drought patterns over East Africa.
737 *Earth's Future*, 8(7), e2020EF001502. <https://doi.org/10.1029/2020EF001502>.

738 Hansen M.C., Defries R.S., Townshend R.G., and Sohlberg R., 2000. Global land cover
739 classification at 1 km spatial resolution using a classification tree approach. *Int. J. Remote Sens.*,
740 21, 1331–1364. <https://doi.org/10.1080/014311600210209>.

741 Hay L.E., Wilby R.L. and Leavesley G.H., 2000. A comparison of delta change and downscaled
742 GCM scenarios for three mountainous basins in the United States. *J. Am. Water Resour. Assoc.*,
743 36(2), 387–397. <https://doi.org/10.1111/j.1752-1688.2000.tb04276.x>.

744 Hayes M.J., Svoboda M.D., Wilhite D.A., Vanyarkho, O.V., 1999. Monitoring the 1996 drought
745 using the standardized precipitation index. *Bull. Am. Meteorol. Soc.*, 80(3), 429–438.
746 [https://doi.org/10.1175/1520-0477\(1999\)080<0429:MTDUTS>2.0.CO;2](https://doi.org/10.1175/1520-0477(1999)080<0429:MTDUTS>2.0.CO;2).

747 Hayes M, Svoboda M, Wall N, and Widhalm M, 2011. The Lincoln Declaration on Drought Indices:
748 Universal Meteorological Drought Index Recommended. *Bull. Am. Meteorol. Soc.*, 92(4), 485–
749 488. <https://doi.org/10.1175/2010BAMS3103.1>.

750 Heim R.R Jr., 2002. A review of twentieth-century drought indices used in the United States. *Bull.*
751 *Am. Meteorol. Soc.*, 83(8), 1149–1165. <https://doi.org/10.1175/1520-0477-83.8.1149>.

752 Huang D.Q., Zhu J., Zhang Y.C., Huang A.N., 2013. Uncertainties on the simulated summer
753 precipitation over Eastern China from the CMIP5 models. *J. Geophys. Res. Atmos.*, 118 (16),
754 9035–9047. <https://doi.org/10.1002/jgrd.50695>.

755 Huang S.Z., Chang J.X., Huang, Q., Chen, Y.T., 2014. Spatio-temporal Changes and Frequency
756 Analysis of Drought in the Wei River Basin, China. *Water Resour. Manag.*, 28(10), 3095–3110.
757 <https://doi.org/10.1007/s11269-014-0657-4>.

758 Huang J., Ji M., Xie Y., Wang S., He Y., and Ran J., 2016. Global semi-arid climate change over last
759 60 years. *Climate Dyn.*, 46, 1131–1150. <https://doi.org/10.1007/s00382-015-2636-8>.

760 Huang J.L., Zhai J.Q., Jiang T., Wang Y.J., Li X.C., Wang R., Xiong M., Su B.D., Fischer T., 2018.
761 Analysis of future drought characteristics in China using the regional climate model CCLM.
762 *Clim. Dyn.*, 50(1-2), 507–525. <https://doi.org/10.1007/s00382-017-3623-z>.

763 Hollinger S.E., Isard S.A., Welford M.R., 1993. A new soil moisture drought index for predicting
764 crop yields. In: Preprints, Eighth Conf. on Applied Climatology, Anaheim, CA, Am Meteor
765 Soc, pp. 187–190.

766 Hosseinzadehtalaei P., Tabari H. & Willems P., 2017. Uncertainty assessment for climate change
767 impact on intense precipitation: How many model runs do we need? *Int. J. Climatol.*, 37, 1105–
768 1117. <https://doi.org/10.1002/joc.5069>.

769 IPCC. Climate Change 2007: The physical science basis[M]. Cambridge: Cambridge University
770 Press, 2007.

771 IPCC (2013) Climate Change 2013: The Physical Science Basis. Contribution of Working Group I
772 to the Fifth Assessment Report of the Intergovernmental Panel on Climate Change [Stocker TF,

773 Qin D, Plattner G-K, Tignor M, Allen SK, Boschung J, Nauels A, Xia Y, Bex V, Midgley PM
774 (eds)]. Cambridge University Press: Cambridge, United Kingdom and New York, NY, USA,
775 pp 1535. <https://doi.org/10.1017/CBO9781107415324>.

776 Jeong D.I., Sushama L. & Naveed Khaliq M., 2014. The role of temperature in drought projections
777 over North America. *Clim. Change*, 127, 289–303. [https://doi.org/10.1007/s10584-014-1248-](https://doi.org/10.1007/s10584-014-1248-3)
778 [3](https://doi.org/10.1007/s10584-014-1248-3).

779 Ju J.L., Dai H., Wu C.H., Hu B.X., Ye M., Chen X.Y., Gui D.W., Liu H.F. and Zhang J., 2021.
780 Quantifying the Uncertainty of the Future Hydrological Impacts of Climate Change: Comparative
781 Analysis of an Advanced Hierarchical Sensitivity in Humid and Semiarid Basins. *J. Hydrometeorol.*,
782 DOI: <https://doi.org/10.1175/JHM-D-20-0016.1>.

783 Jung I.W., Chang H.J., and Moradkhani H., 2011. Quantifying uncertainty in urban flooding analysis
784 considering hydro-climatic projection and urban development effects. *Hydrol. Earth Syst. Sci.*,
785 15, 617–633. <https://doi.org/10.5194/hess-15-617-2011>.

786 Kay A.L., Davies H.N., Bell V.A., Jones R.G., 2009. Comparison of uncertainty sources for climate
787 change impacts: flood frequency in England. *Clim. Change*, 92(1-2), 41–63.
788 <https://doi.org/10.1007/s10584-008-9471-4>.

789 Keyantash J., and Dracup J. A., 2002. The quantification of drought: An evaluation of drought
790 indices. *Bull. Amer. Meteor. Soc.*, 83(8), 1167–1180. [https://doi.org/10.1175/1520-0477-](https://doi.org/10.1175/1520-0477-83.8.1167)
791 [83.8.1167](https://doi.org/10.1175/1520-0477-83.8.1167).

792 Kharin V.V., Zwiers F.W., Zhang X., Wehner M., 2013. Changes in temperature and precipitation
793 extremes in the CMIP5 ensemble. *Clim. Change*, 119, 345–357.
794 <https://doi.org/10.1007/s10584-013-0705-8>.

795 Kim S., Eghdamirad S., Sharma A. & Kim, J.H., 2020. Quantification of uncertainty in projections
796 of extreme daily precipitation. *Earth and Space Science*, 7(8), e2019EA001052.
797 <https://doi.org/10.1029/2019EA001052>.

798 Lafon T., Dadson S., Buys G. and Prudhomme C., 2013. Bias correction of daily precipitation
799 simulated by a regional climate model: a comparison of methods. *Int. J. Climatol.*, 33, 1367–
800 1381. <https://doi.org/10.1002/joc.3518>.

801 Lee M.H., Im E.S., Bae D.H., 2019. A comparative assessment of climate change impacts on drought
802 over Korea based on multiple climate projections and multiple drought indices. *Clim. Dyn.*, 53,
803 389–404. <https://doi.org/10.1007/s00382-018-4588-2>.

804 Li Z., Zheng F., Liu W., 2012. Spatiotemporal characteristics of reference evapotranspiration during
805 1961-2009 and its projected changes during 2011-2099 on the Loess Plateau of China. *Agric.*
806 *For. Meteorol.*, 154-155, 147–155. <https://doi.org/10.1016/j.agrformet.2011.10.019>.

807 Liang X., Lettenmaier D.P., Wood E.F., and Burges S.J., 1994. A simple hydrologically based model
808 of land surface water and energy fluxes for general circulation models. *J. Geophys. Res.*, 99(D7),
809 14415–14428. <https://doi.org/10.1029/94JD00483>.

810 Liang X., Lettenmaier D.P., Wood E.F., 1996. Surface soil moisture parameterization of the VIC-2L
811 model: Evaluation and modification. *Glob. Planet. Chang.*, 13(1-4): 195–206. [https://doi.org/](https://doi.org/10.1016/0921-8181(95)00046-1)
812 [10.1016/0921-8181\(95\)00046-1](https://doi.org/10.1016/0921-8181(95)00046-1).

813 Mckee T.B., Doesken N.J., Kleist J. The relationship of drought frequency and duration to time
814 scales. In: Eighth conference on applied climatology, American meteorological society,
815 Anaheim, CA;1993.

816 Mishra A.K., Desai V.R., 2005. Drought forecasting using stochastic models. *Stoch. Env. Res. Risk*

817 A. 19(5), 326–339. <https://doi.org/10.1007/s00477-005-0238-4>.

818 Mishra A.K., Singh V.P., 2010. A review of drought concepts. *J. Hydrol.*, 391(1-2), 202–216.

819 <https://doi.org/10.1016/j.jhydrol.2010.07.012>.

820 Mishra A.K., Singh V.P., 2011. Drought modeling—A review. *J. Hydrol.*, 403(1-2), 157–175.

821 <https://doi.org/10.1016/j.jhydrol.2011.03.049>.

822 Mo K.C., 2008. Model-Based Drought Indices over the United States. *J. Hydrometeorol.*, 9(6),

823 1212–1230. <https://doi.org/10.1175/2008JHM1002.1>.

824 Moss R.H. and Coauthors, 2010. The next generation of scenarios for climate change research and

825 assessment. *Nature*, 463, 747–756. <https://doi.org/10.1038/nature08823>.

826 Nakićenović N. and Coauthors, 2000. *Special Report on Emissions Scenarios (SRES): A Special*

827 *Report of Working Group III of the Intergovernmental Panel on Climate Change*. N.

828 Nakićenović and R. Swart, Eds., Cambridge University Press, 570 pp.

829 Niu J., Chen J., Sun L., 2015. Exploration of drought evolution using numerical simulations over

830 the Xijiang (West River) basin in South China. *J. Hydrol.*, 526, 68–77.

831 <https://doi.org/10.1016/j.jhydrol.2014.11.029>.

832 Orłowsky B., Seneviratne S.I., 2013. Elusive drought: uncertainty in observed trends and short- and

833 long-term CMIP5 projections. *Hydrol. Earth Syst. Sci.* 17(5), 1765–1781.

834 <https://doi.org/10.5194/hess-17-1765-2013>.

835 Palmer W. Meteorological drought, Weather Bur. Res. Rep. 45. US Department of Agriculture, US

836 Gov. Print. Off., Washington, DC, 1965.

837 Palmer W.C., 1968. Keeping track of crop moisture conditions, nationwide: the new crop moisture

838 index. *Weatherwise*, 21(4), 156–161. <https://doi.org/10.1080/00431672.1968.9932814>.

839 Peters G, Bier G, van Lanen H.A.J., Torfs P.J.J.F., 2006. Propagation and spatial distribution of

840 drought in a groundwater catchment. *J. Hydrol.*, 321(1-4), 257–275.

841 <https://doi.org/10.1016/j.jhydrol.2005.08.004>.

842 Piao S.L., Ciais P., Huang Y., Shen Z.H., Li S.J., Zhou L.P. et al., 2010. The impacts of climate

843 change on water resources and agriculture in China. *Nature*, 467(7311), 43–51,

844 <https://doi.org/10.1038/nature09364>.

845 Rhee J.Y., and Cho J., 2016. Future Changes in Drought Characteristics: Regional Analysis for

846 South Korea under CMIP5 projections. *J. Hydrometeorol.*, 17, 437–451.

847 <https://doi.org/10.1175/JHM-D-15-0027.1>.

848 Rudd A.C., Kay A.L., Bell V.A., 2019. National-scale analysis of future river flow and soil moisture

849 droughts: potential changes in drought characteristics. *Clim. Change*, 156(3), 323–340.

850 <https://doi.org/10.1007/s10584-019-02528-0>.

851 Ruosteenoja K., Markkanen T., Venalainen A., Raisanen P., Peltola H., 2018. Seasonal soil moisture

852 and drought occurrence in Europe in CMIP5 projections for the 21st century. *Clim. Dyn.*, 50(3-

853 4), 1177–1192. <https://doi.org/10.1007/s00382-017-3671-4>.

854 Samaniego L., Thober S., Kumar R., Wanders N., Rakovec O., Pan M., Zink M., Sheffield J., Wood

855 E., and Marx A., 2018. Anthropogenic warming exacerbates European soil moisture droughts.

856 *Nat. Clim. Change*, 8(5), 421–426. <https://doi.org/10.1038/s41558-018-0138-5>.

857 Saxton, K.E., Rawls, W.J., 2006. Soil water characteristic estimates by texture and organic matter

858 for hydrologic solutions. *Soil Sci. Soc. Am. J.*, 70 (5), 1569–1578.

859 <https://doi.org/10.2136/sssaj2005.0117>.

860 Shafer B.A., Dezman L.E., 1982. Development of a Surface Water Supply Index (SWSI) to Assess

861 the Severity of Drought Conditions in Snowpack Runoff Areas. In: Preprints, Western
862 SnowConf., Reno, NV, Colorado State University, pp. 164–175.

863 Sheffield J., Wood E.F., 2008. Projected changes in drought occurrence under future global warming
864 from multi-model, multi-scenario, IPCC AR4 simulations. *Clim. Dyn.*, 31(1), 79–105.
865 <https://doi.org/10.1007/s00382-007-0340-z>.

866 Shukla S., Wood A.W., 2008. Use of a standardized runoff index for characterizing hydrologic
867 drought. *Geophys. Res. Lett.*, 35(2), L02405. <https://doi.org/10.1029/2007GL032487>.

868 Sillmann J, Kharin V.V., Zwiers F.W., Zhang X. and Bronaugh D., 2013. Climate extremes indices
869 in the CMIP5 multimodel ensemble: Part 2. Future climate projections. *J. Geophys. Res. Atmos.*,
870 118, 2473–2493. <https://doi.org/10.1002/jgrd.50188>.

871 Sperna Weiland F.C., Van Beek L.P.H., Kwadijk J.C.J., Bierkens M.F.P., 2010. The ability of a
872 GCM-forced hydrological model to reproduce global discharge variability. *Hydrol. Earth Syst.
873 Sci.*, 14, 1595–1621. <https://doi.org/10.5194/hess-14-1595-2010>.

874 Su B.D., Huang J.L., Zeng X.F., Gao C., Jiang T., 2017. Impacts of climate change on streamflow
875 in the upper Yangtze River basin. *Clim. Change*, 141(3), 533–546.
876 <https://doi.org/10.1007/s10584-016-1852-5>.

877 Tallaksen L.M., Hisdal H, van Lanen H.A.J., 2009. Space-time modelling of catchment scale
878 drought characteristics. *J. Hydrol.*, 375(3-4), 363–372.
879 <https://doi.org/10.1016/j.jhydrol.2009.06.032>.

880 Thibeault J.M., and Seth A., 2014. Changing climate extremes in the Northeast United States:
881 Observations and projections from CMIP5. *Clim. Change*, 127(2), 273–287.
882 <https://doi.org/10.1007/s10584-014-1257-2>.

883 Thornton P.K., Ericksen P., Herrero M., Challinor A.J., 2014. Climate variability and vulnerability
884 to climate change: a review. *Global Change Biol.*, 20, 3313–3328,
885 <https://doi.org/10.1111/gcb.12581>.

886 Touma D., Ashfaq M., Nayak M.A., Kao S.C., Diffenbaugh N.S., 2015. A multi-model and multi-
887 index evaluation of drought characteristics in the 21st century. *J. Hydrol.*, 526, 196–207.
888 <https://doi.org/10.1016/j.jhydrol.2014.12.011>.

889 Trenberth K.E., Dai A., Van Der Schrier G., Jones P.D., Barichivich J., Briffa K.R., and Sheffield J.,
890 2014, Global warming and changes in drought, *Nat. Clim. Change*, 4, 17–22,
891 <https://doi.org/10.1038/nclimate2067>.

892 Ukkola A.M., Pitman A.J., De Kauwe M.G., Abramowitz G., Herger N., Evans J.P., Decker M.,
893 2018. Evaluating CMIP5 Model Agreement for Multiple Drought Metrics. *J. Hydrometeorol.*,
894 19(6), 969–988. <https://doi.org/10.1175/JHM-D-17-0099.1>.

895 Van Rooy M.P., 1965. A rainfall anomaly index independent of time and space. *Notos*, 14, 43.

896 van Vuuren D.P., and Coauthors, 2011. The representative concentration pathways: An overview.
897 *Clim. Change*, 109, 5–31. <https://doi.org/10.1007/s10584-011-0148-z>.

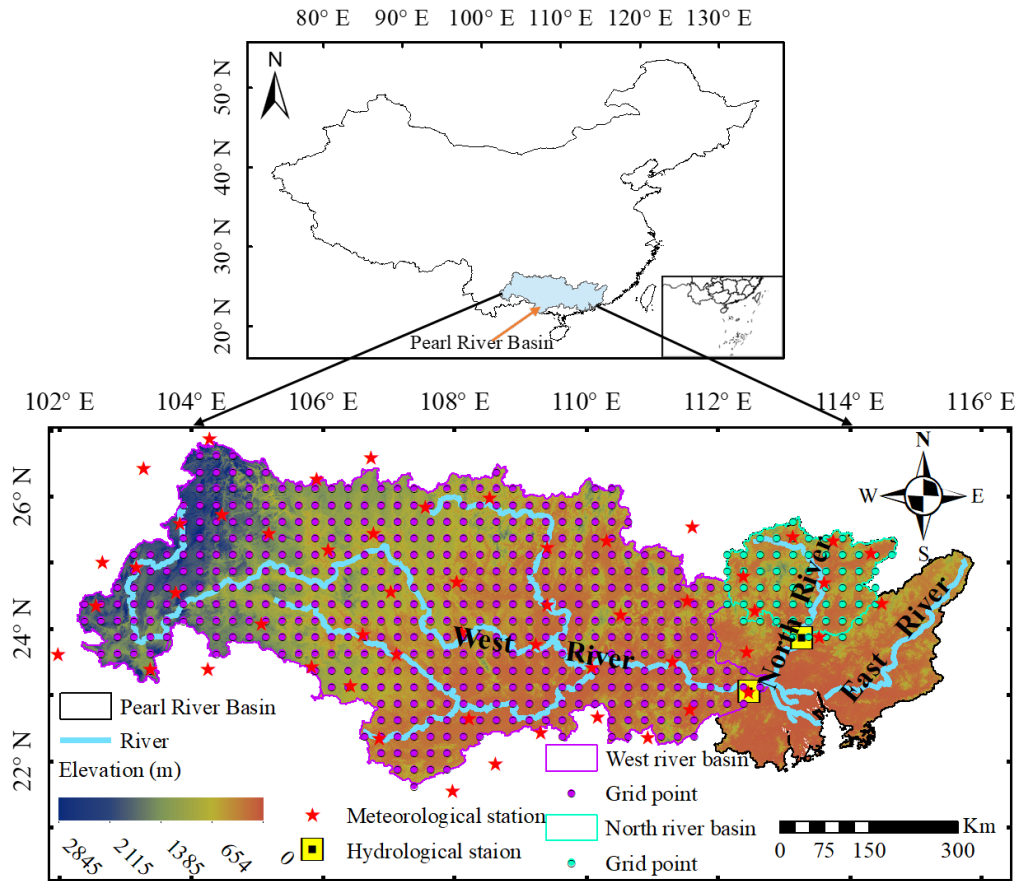
898 Venkataraman K., Tummuri S., Medina A., Perry J., 2016. 21st century drought outlook for major
899 climate divisions of Texas based on CMIP5 multimodel ensemble: Implications for water
900 resource management. *J. Hydrol.*, 534, 300–316. <https://doi.org/10.1016/j.jhydrol.2016.01.001>.

901 Vetter T., Reinhardt J., Flörke M., Griensven A.V., Hattermann F., Huang S.C., et al. 2017.
902 Evaluation of sources of uncertainty in projected hydrological changes under climate change
903 in 12 large-scale river basins. *Clim. Change*, 141(3), 419–433. <https://doi.org/10.1007/s10584-016-1794-y>.

- 905 Vicente-Serrano S.M., Beguería S., López-Moreno J.I., 2010. A multiscalar drought index sensitive
 906 to global warming: the standardized precipitation evapotranspiration index. *J. Clim.*, 23(7),
 907 1691–1718. <https://doi.org/10.1175/2009JCLI2909.1>.
- 908 von Buttlar J., Zscheischler J., Ramming A., Sippel S., Reichstein M., Knohl A. et al., 2018. Impacts
 909 of droughts and extreme-temperature events on gross primary production and ecosystem
 910 respiration: A systematic assessment across ecosystems and climate zones. *Biogeosciences*,
 911 15(5), 1293–1318. <https://doi.org/10.5194/bg-15-1293-2018>.
- 912 Wang G.L., 2005. Agricultural drought in a future climate: results from 15 global climate models
 913 participating in the IPCC 4th assessment. *Clim. Dyn.*, 25(7-8), 739–753.
 914 <https://doi.org/10.1007/s00382-005-0057-9>.
- 915 Wang L., Chen W., 2014. A CMIP5 multimodel projection of future temperature, precipitation, and
 916 climatological drought in China. *Int. J. Climatol.*, 34(6), 2059–2078.
 917 <https://doi.org/10.1002/joc.3822>.
- 918 Wang Z.L., Zhong R.D., Lai C.G., Zeng Z.Y., Lian Y.Q., Bai X.Y., 2018. Climate change enhances
 919 the severity and variability of drought in the Pearl River Basin in South China in the 21st
 920 century. *Agric. For. Meteorol.*, 249, 149–162. <https://doi.org/10.1016/j.agrformet.2017.12.077>.
- 921 Wells, N., Goddard, S., Hayes, M.J., 2004. A self-Calibrating palmer drought severity index. *J. Clim.*,
 922 17(12), 2335–2351. <https://doi.org/10.1175/JCLI17122335>.
- 923 Wilby R.L. and Harris I., 2006. A framework for assessing uncertainties in climate change impacts:
 924 Low-flow scenarios for the River Thames, UK. *Water Resour. Res.*, 42(2), W02419.
 925 <https://doi.org/10.1029/2005wr004065>.
- 926 Wilhite D.A., Glantz M.H., 1985. Understanding: the drought phenomenon: the role of definitions.
 927 *Water Int.*, 10(3), 111–120. <https://doi.org/10.1080/02508068508686328>.
- 928 Wilhite D.A., 2000. Drought as a natural hazard: concepts and definitions. In: Wilhite D.A.(Ed.),
 929 Drought: A Global Assessment, Hazard Disasters Ser, vol. 1. Routledge, New York, USA, pp.
 930 3–18.
- 931 World Meteorological Organization (WMO) and Global Water Partnership (GWP) (2016) In
 932 tegrated drought management programme handbook of drought indicators and indices.
 933 No. 1173. http://www.droughtmanagement.info/literature/GWP_Handbook_of_Drought_Indicators_and_Indices_2016.pdf.
- 934 http://www.droughtmanagement.info/literature/GWP_Handbook_of_Drought_Indicators_and_Indices_2016.pdf.
- 935 Woldemeskel F.M., Sharma A., Sivakumar B. & Mehrotra R., 2016. Quantification of precipitation
 936 and temperature uncertainties simulated by CMIP3 and CMIP5 models. *J. Geophys. Res. Atmos.*,
 937 121(1), 3–17. <https://doi.org/10.1002/2015JD023719>.
- 938 Wu Z.Y., Lu G.H., Liu Z.Y., Wang J.X., Xiao H., 2013. Trends of extreme flood events in the Pearl
 939 River Basin during 1951-2010. 4(2), 110–116. <https://doi.org/10.3724/SP.J.1248.2013.110>.
- 940 Wu C.H. & Huang G.R., 2014. Changes in heavy precipitation and floods in the upstream of the
 941 Beijiang River basin, South China. *Int. J. Climatol.* 35, 2978–2992.
 942 <https://doi.org/10.1002/joc.4187>.
- 943 Wu C.H., Huang G.R., Yu H.J., Chen Z.J., and Ma J.G., 2014. Impact of climate change on reservoir
 944 flood control in the upstream area of the Beijiang River Basin, South China. *J. Hydrometeorol.*,
 945 15(6), 2203–2218. <https://doi.org/10.1175/JHM-D-13-0181.1>.
- 946 Wu C.H., Huang G.R., and Yu H.J., 2015. Prediction of extreme floods based on CMIP5 climate
 947 models: A case study in the Beijiang River basin, South China. *Hydrol. Earth Syst. Sci.*, 19(3),
 948 1385–1399. <https://doi.org/10.5194/hess-19-1385-2015>.

- 949 Wu C.H., Xian Z.Y., Huang G.R., 2016. Meteorological drought in the Beijiang River basin, South
950 China: current observations and future projections. *Stoch. Environ. Res. Risk Assess.*, 30(7),
951 1821–1834. <https://doi.org/10.1007/s00477-015-1157-7>.
- 952 Wu C.H. and Huang G.R., 2016. Projection of climate extremes in the Zhujiang River basin using
953 a regional climate model. *Int. J. Climatol.*, 36(3), 1184–1196. <https://doi.org/10.1002/joc.4412>.
- 954 Wu C.H., Yeh Pat J.-F., Chen Y.Y., Hu Bill X., Huang G.R., 2020. Future precipitation-driven
955 meteorological drought changes in the CMIP5 multi-model ensembles under 1.5°C and 2°C
956 global warming. *J. Hydrometeorol.*, 21(9), 2177–2196. <https://doi.org/10.1175/JHM-D-19-0299.1>.
- 957
- 958 Wu C.H., Yeh P.J.-F., Ju J.L., Chen Y.Y., Xu K., Dai H., Niu J., Hu B.X., and Huang G.R. 2021.
959 Assessing the spatio-temporal uncertainties in future meteorological droughts from CMIP5
960 models, emission scenarios and bias corrections. *J. Climate*, 34(5), 1903–1922, <https://doi.org/10.1175/JCLI-D-20-0411.1>.
- 961
- 962 Xiao M.Z., Zhang Q., Singh V.P., Liu L., 2016. Transitional properties of droughts and related
963 impacts of climate indices in the Pearl River basin, China. *J. Hydrol.*, 534, 397–406.
964 <https://doi.org/10.1016/j.jhydrol.2016.01.012>.
- 965 Xu K., Qin G.X., Niu J., Wu C.H., Hu B.X., Huang G.R., and Wang P., 2019a. Comparative analysis
966 of meteorological hydrological drought over the Pearl River basin in southern China. *Hydrol.*
967 *Res.*, 50(1), 301–318. <https://doi.org/10.2166/nh.2018.178>.
- 968 Xu K., Xu B.B., Ju J.L., Wu C.H., Dai H. and Hu B.X., 2019b. Projection and uncertainty of
969 precipitation extremes in the CMIP5 multimodel ensembles over nine major basins in China.
970 *Atmos. Res.*, 226(15), 122–137. <https://doi.org/10.1016/j.atmosres.2019.04.018>.
- 971 Xu K., Wu C.H. & Hu B.X., 2019c. Projected changes of temperature extremes over nine major
972 basins in China based on the CMIP5 multimodel ensembles. *Stoch. Environ. Res. Risk Assess.*,
973 33, 321–339. <https://doi.org/10.1007/s00477-018-1569-2>.
- 974 Yan D., Werners S.E., Ludwig F., Huang Q.H., 2015. Hydrological response to climate change: The
975 Pearl River, China under different RCP scenarios. *J. Hydrol. Reg. Stud.*, 4, 228–245.
976 <https://doi.org/10.1016/j.ejrh.2015.06.006>.
- 977 Yang T., Ding J., Liu D., Wang X. & Wang T., 2019. Combined use of multiple drought indices for
978 global assessment of dry gets drier and wet gets wetter paradigm. *J. Clim.*, 32(3), 737– 748.
979 <https://doi.org/10.1175/JCLI-D-18-0261.1>.
- 980 Yao N., Li L.C., Feng P.Y., Feng H., Liu D.L., Liu Y., Jiang K.T., Jiang K.T., Hu X.T., Li Y., 2020.
981 Projections of drought characteristics in China based on a standardized precipitation and evap
982 otranspiration index and multiple GCMs. *Sci. Total Environ.*, 704, 135245.
983 <https://doi.org/10.1016/j.scitotenv.2019.135245>.
- 984 Yoo J.Y., Kwon H.H., Lee J.H. & Kim T.W., 2016. Influence of evapotranspiration on future drought
985 risk using bivariate drought frequency curves. *KSCE J. Civ. Eng.*, 20(5), 2059–2069.
986 <https://doi.org/10.1007/s12205-015-0078-9>.
- 987 Zarekarizi M., Rana A. & Moradkhani H., 2018. Precipitation extremes and their relation to climatic
988 indices in the Pacific Northwest USA. *Clim. Dyn.*, 50, 4519–4537.
989 <https://doi.org/10.1007/s00382-017-3888-2>.
- 990 Zhang S.R., Lu X.X., Higgitt D.L., Chen C.A., Han J.T., Sun H.G., 2008. Recent changes of water
991 discharge and sediment load in the Zhujiang (Pearl River) Basin, China. *Glob. Planet. Change*,
992 60(3-4), 365–380. <https://doi.org/10.1016/j.gloplacha.2007.04.003>.

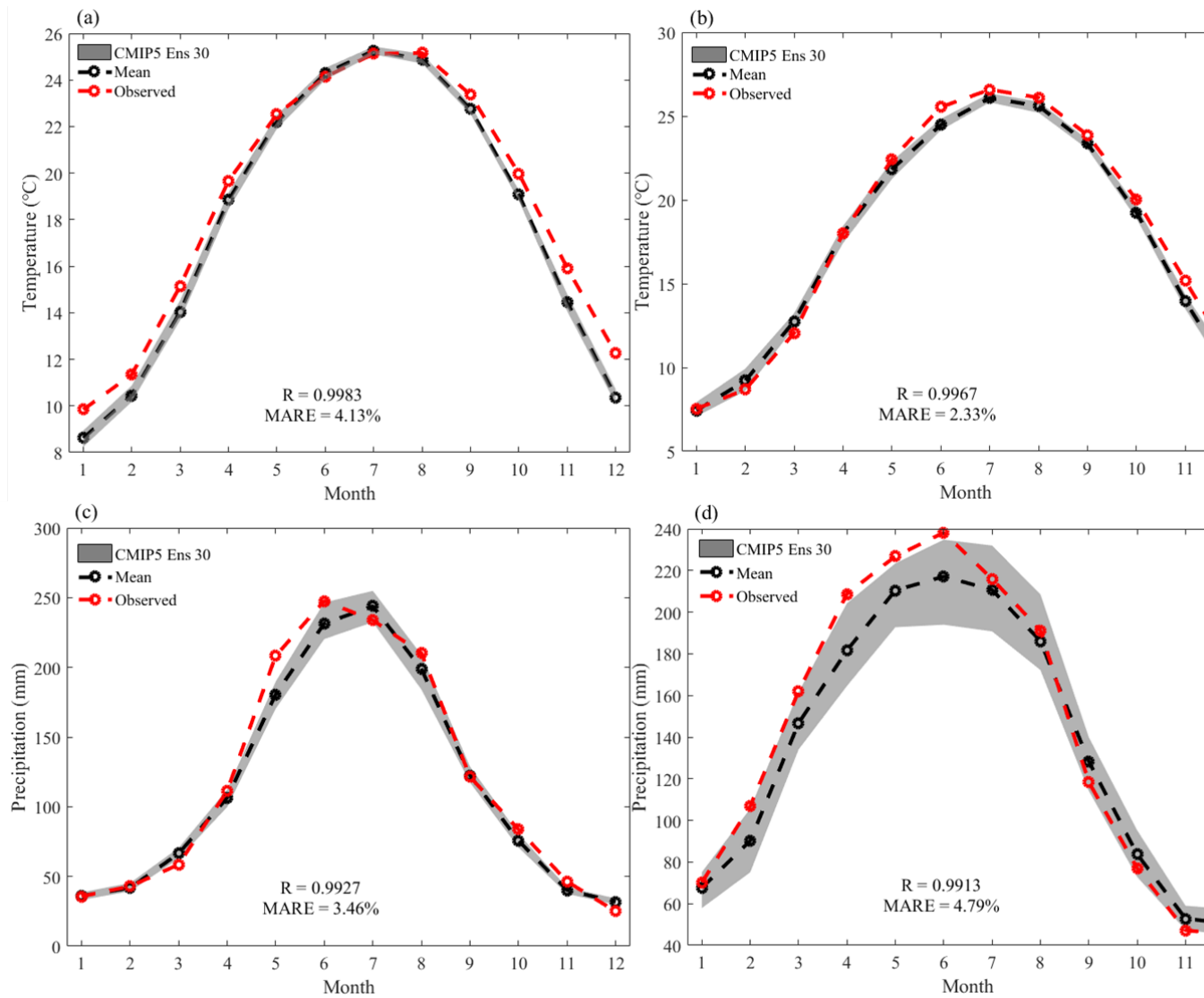
- 993 Zhang Q, Xu C.Y., Zhang Z.X., 2009. Observed changes of drought/wetness episodes in the Pearl
994 River Basin, China, using the Standardized Precipitation Index and Aridity Index. *Theor. Appl.*
995 *Climatol.*, 98, 89–99. <https://doi.org/10.1007/s00704-008-0095-4>.
- 996 Zhang Q., Xiao M.Z., Singh V.P., Li J.F., 2012. Regionalization and spatial changing properties of
997 droughts across the Pearl River basin, China. *J. Hydrol.*, 472-473, 355–366.
998 <https://doi.org/10.1016/j.jhydrol.2012.09.054>.
- 999 Zhang Q., Xiao M.Z., Singh V.P., Chen X.H., 2013a. Copula-based risk evaluation of droughts
1000 across the Pearl River basin, China. *Theor. Appl. Climatol.*, 111(1-2), 119–131.
1001 <https://doi.org/10.1007/s00704-012-0656-4>.
- 1002 Zhang W.J., Jin F.F., Zhao J.X., Qi I., Ren H.L., 2013b. The Possible Influence of a Nonconventional
1003 El Niño on the Severe Autumn Drought of 2009 in Southwest China. *J. Clim.*, 26(21). 8392–
1004 8405. <https://doi.org/10.1175/JCLI-D-12-00851.1>.
- 1005 Zhang Q., Xiao M.Z., Singh, V.P., 2015. Uncertainty evaluation of copula analysis of hydrological
1006 droughts in the East River basin, China. *Glob. Planet. Chang.*, 129, 1–9.
1007 <https://doi.org/10.1016/j.gloplacha.2015.03.001>.
- 1008 Zhao T., Dai A., 2017. Uncertainties in historical changes and future projections of drought. Part II:
1009 model-simulated historical and future drought changes. *Clim. Chang.*, 144, 535–548.
1010 <https://doi.org/10.1007/s10584-016-1742-x>.
- 1011 Zhou B.T., Wen H.Q.Z., Xu Y., and Song C.L., 2014. Projected Changes in Temperature and
1012 Precipitation Extremes in China by the CMIP5 Multimodel Ensembles. *J. Clim.*, 27, 659–6611.
1013 <https://doi.org/10.1175/JCLI-D-13-00761.1>.
- 1014 Zhu Y., Wang W., Singh V.P., Liu Y., 2016. Combined use of meteorological drought indices at
1015 multi-time scales for improving hydrological drought detection. *Sci. Total Environ.*, 571, 1058–
1016 1068. <https://dx.doi.org/10.1016/j.scitotenv.2016.07.096>.
- 1017



1018

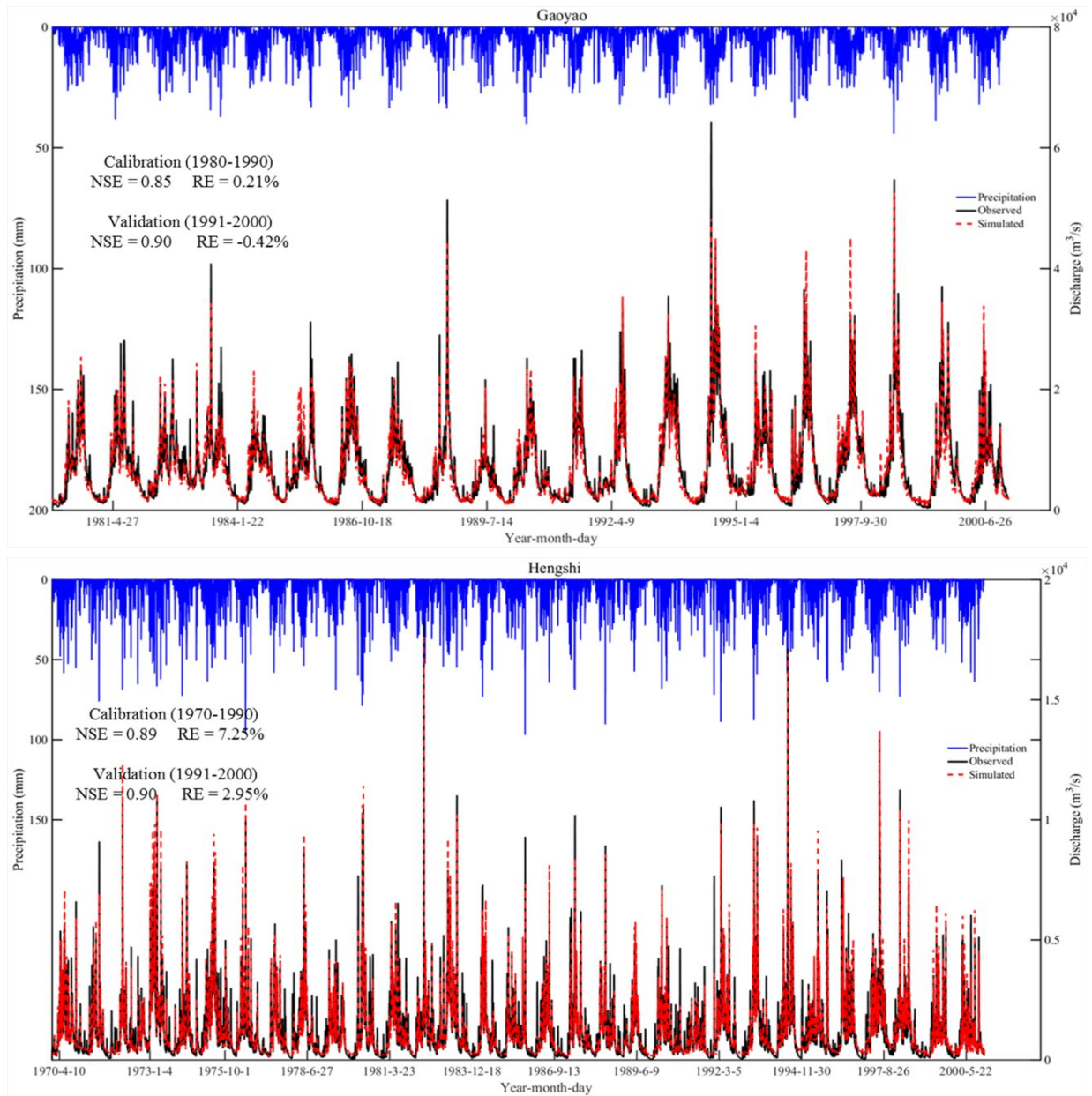
1019 **Fig.1.** Geographical location map of the Pearl River Basin (PRB) as well as the
 1020 distributions of 0.25° grid points and meteorological stations.

1021



1022
 1023
 1024
 1025
 1026
 1027
 1028

Fig.2. Comparisons of the observed (red dotted line) and bias-corrected (grey shadow) monthly T and P of 13 CMIP5 GCMs in the West River (a, c) and North River (b, d) basins for the baseline period 1971-2000. The grey shadow represents the range of 30 samples of bias-corrected simulations of the 13 CMIP5 GCMs. R and MARE indicate correlation coefficient and mean absolute relatively error, respectively.



1029

1030

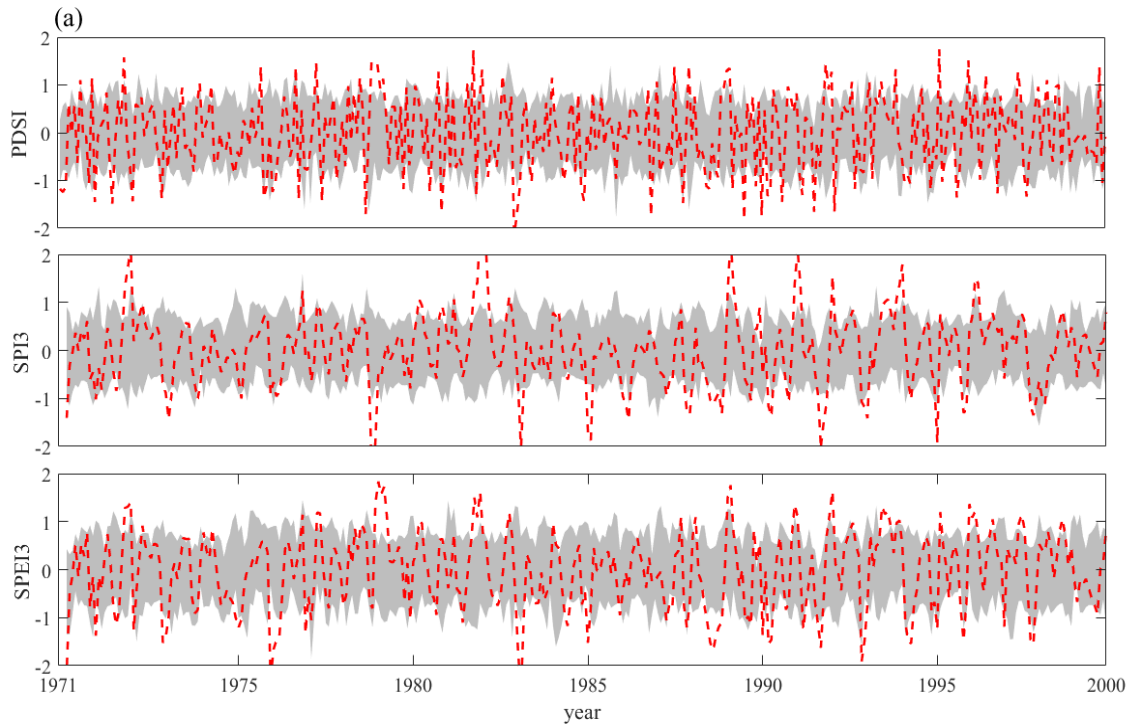
1031

Fig.3. Comparisons of the simulated and observed daily discharges at the Gaoyao (Wet River basin) and Hengshi (North River basin) stations for the calibration and validation periods.

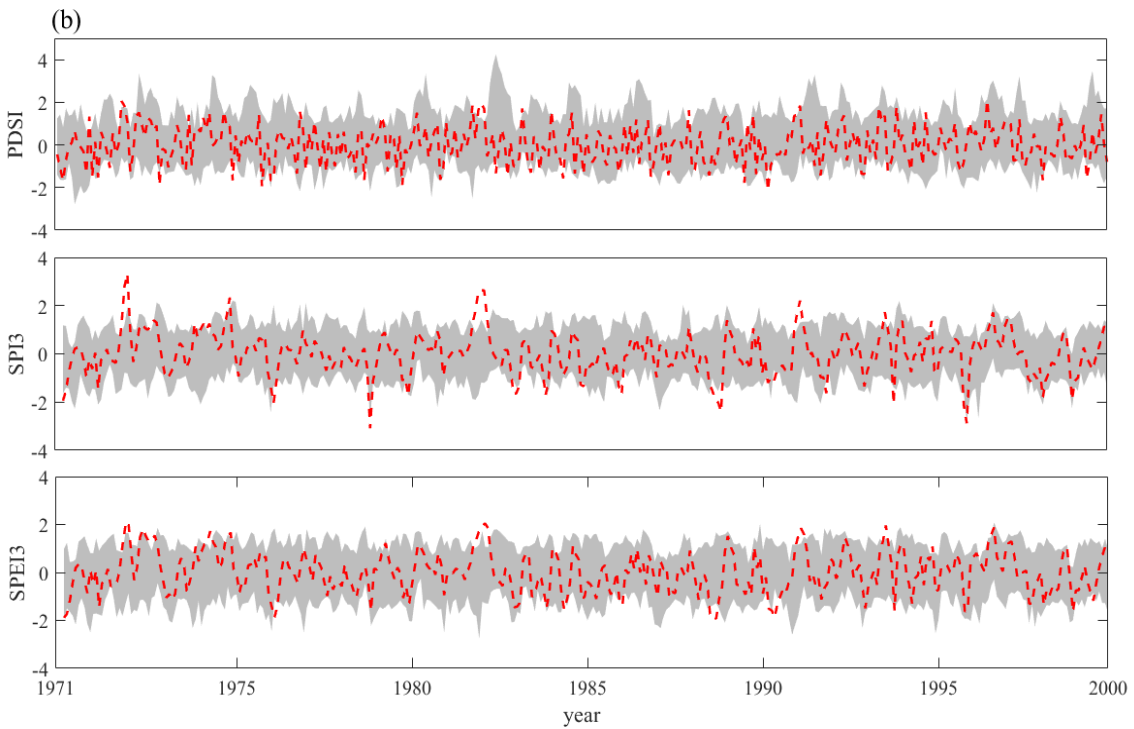
1032

1033

1034

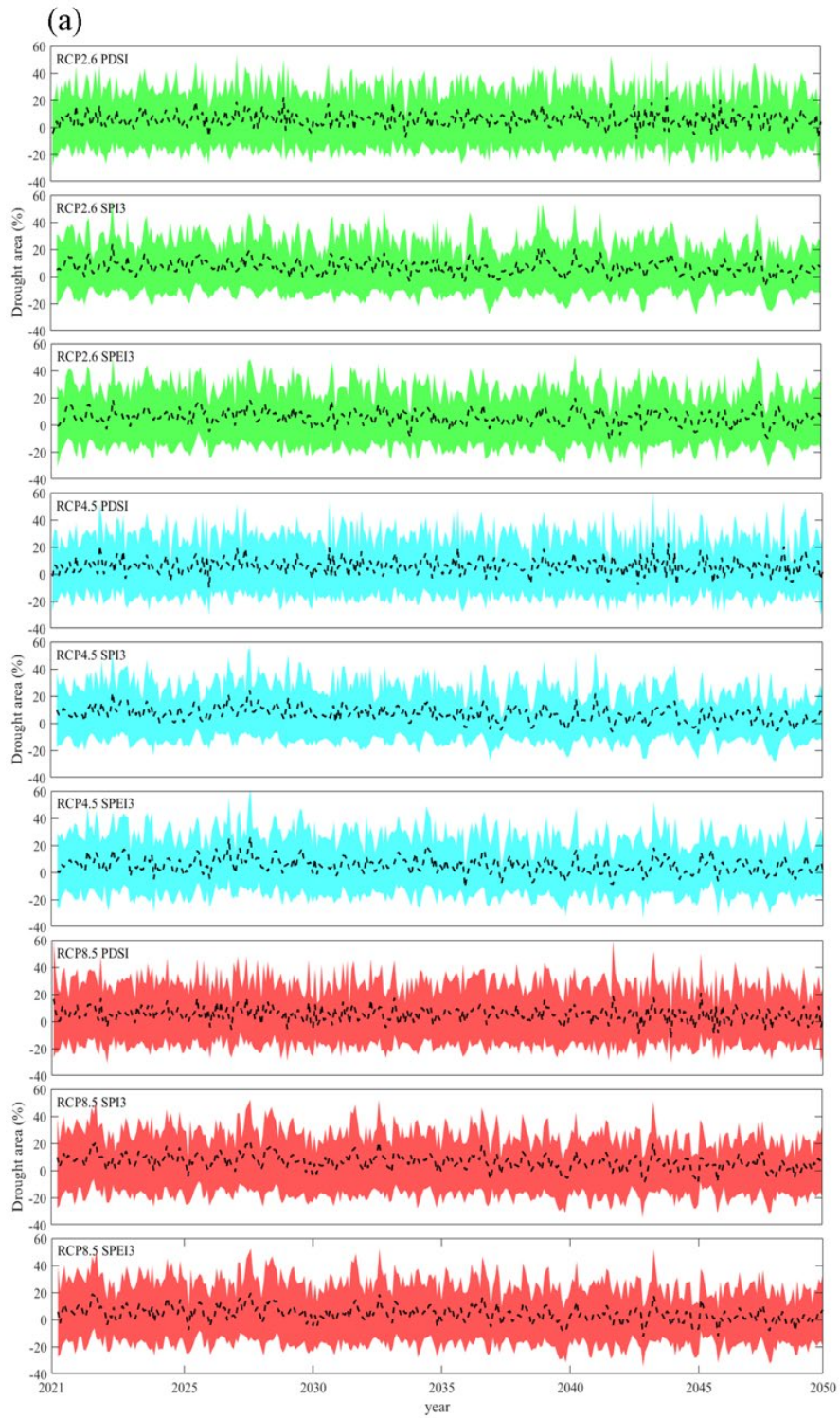


1035

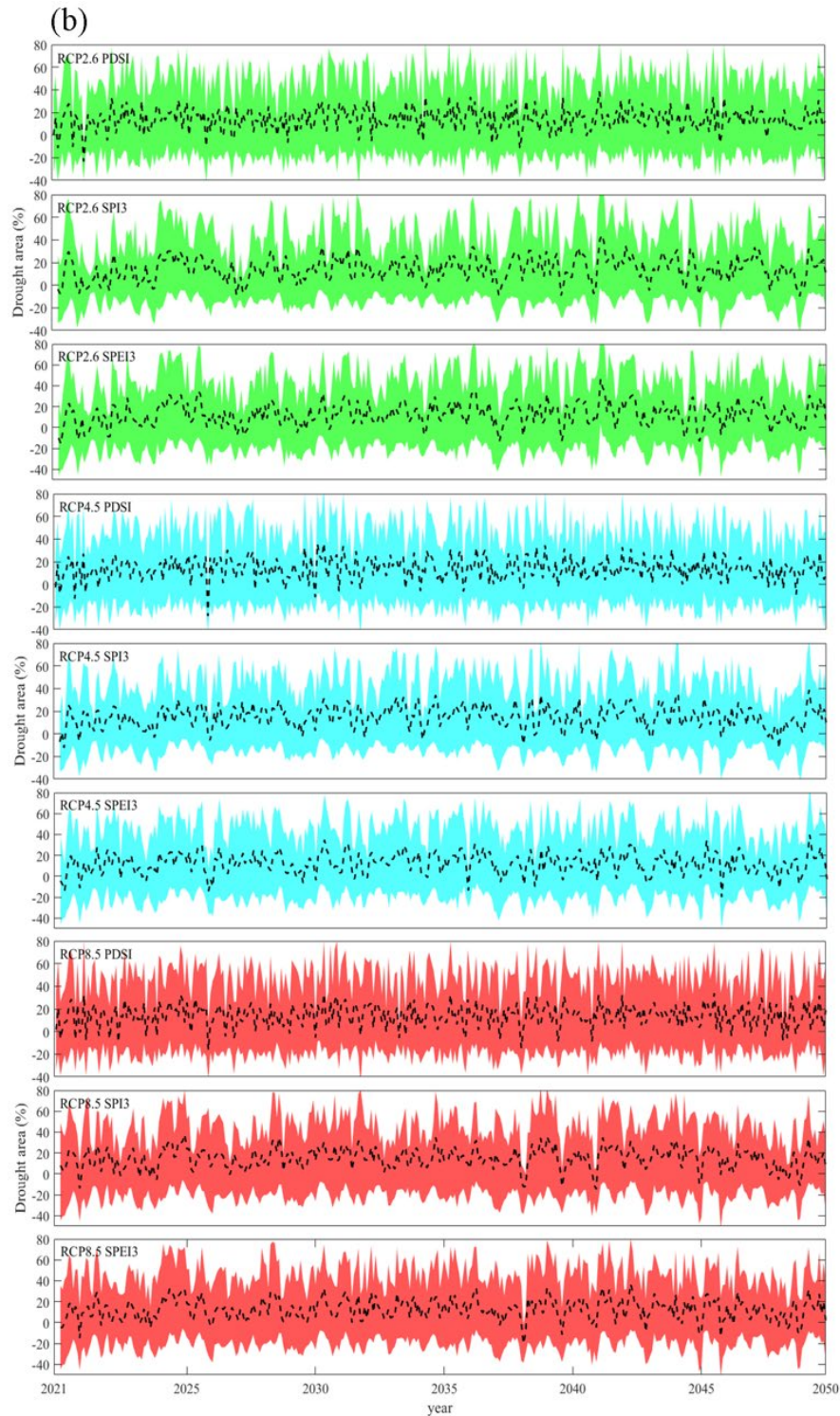


1036

1037 **Fig.4.** Comparisons of the simulated PDSI, SPI3 and SPEI3 (grey shadow)
 1038 with the observed ones (red dotted line) in the West River (a) and North River (b) basins during
 1039 the baseline period 1971-2000. The grey shadow indicates the range of 30 simulation
 1040 samples of PDSI, SPI3 and SPEI3, and the red dotted lines denotes the observed ones.
 1041



1042

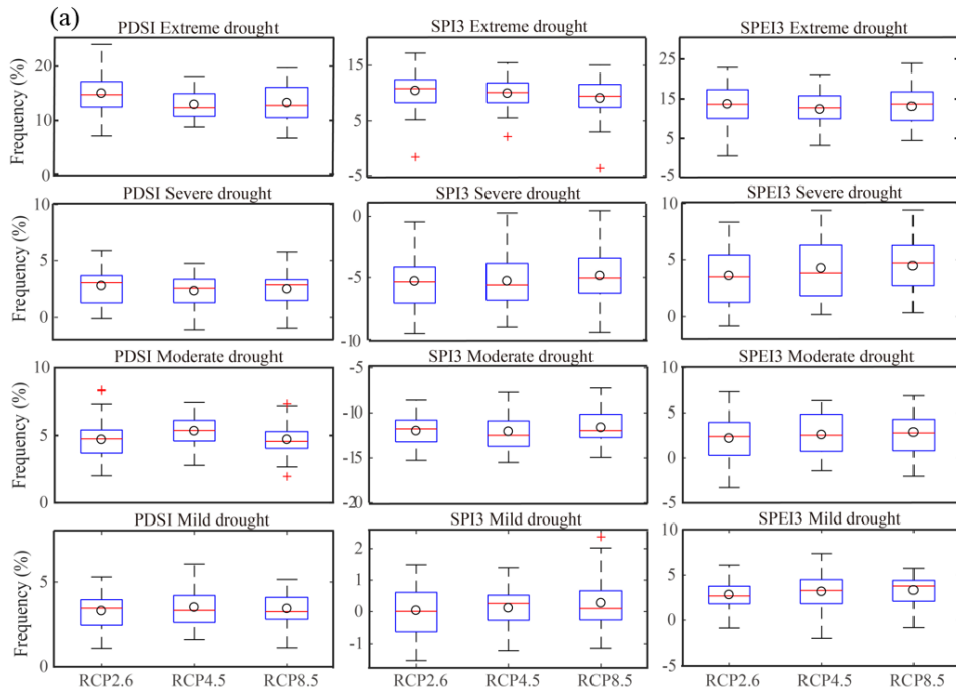


1043

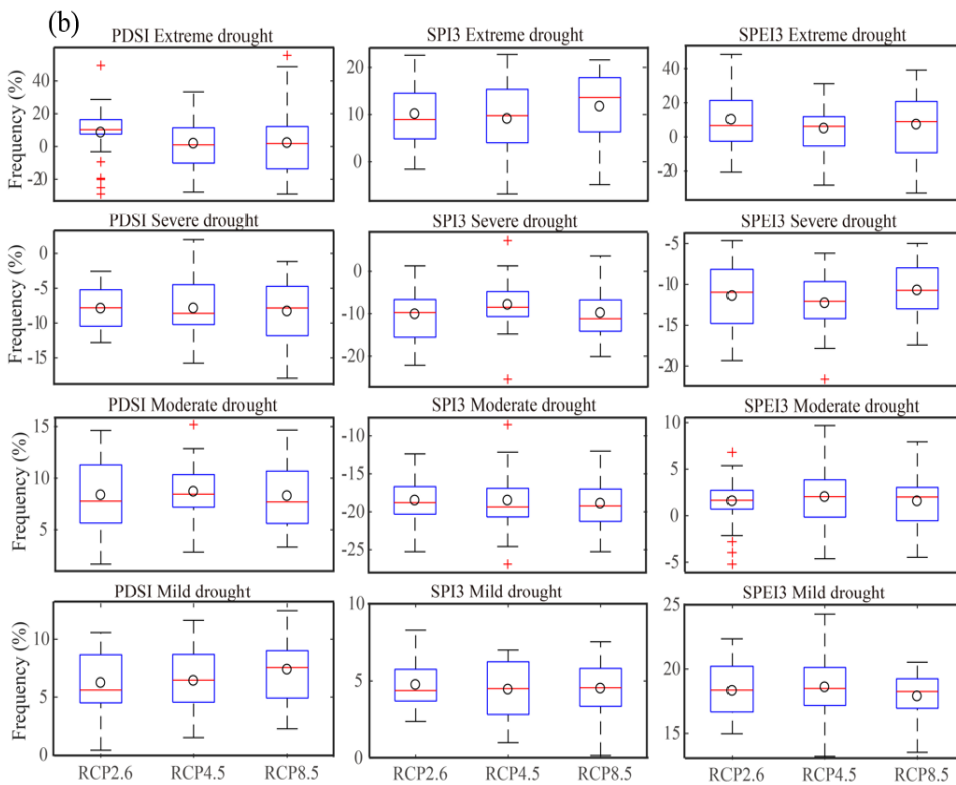
1044 **Fig.5.** Monthly time series of Da (%) indicated by PDSI (≤ -1), SPI3 (≤ -0.5) and SPEI3
 1045 (≤ -0.5) under RCP2.6 (green), RCP4.5 (blue) and RCP8.5 (red) scenarios for the future
 1046 period 2021-2050 (relative to the baseline period 1971-2000) in the West River (a) and
 1047 North River (b) basins. The shadow denotes the range of 30 simulation of 13 CMIP5
 1048 models, and the black lines denotes the ensemble mean of model simulations.

1049

1050

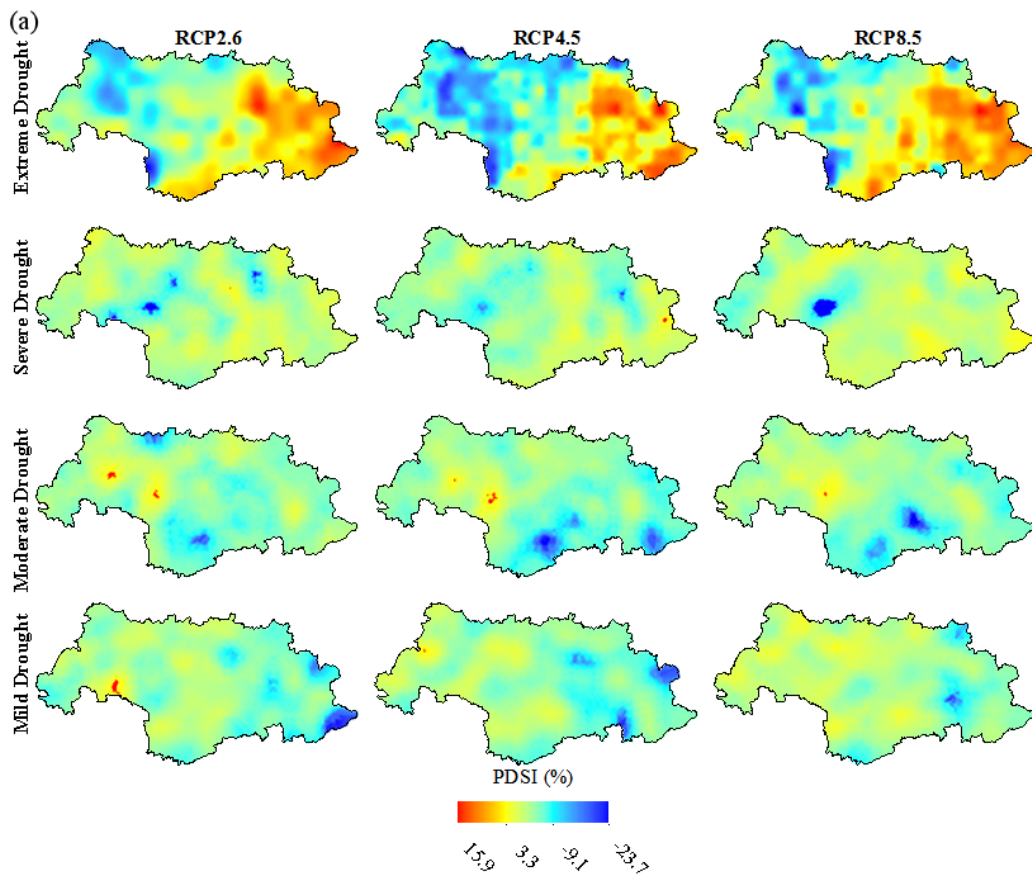


1051

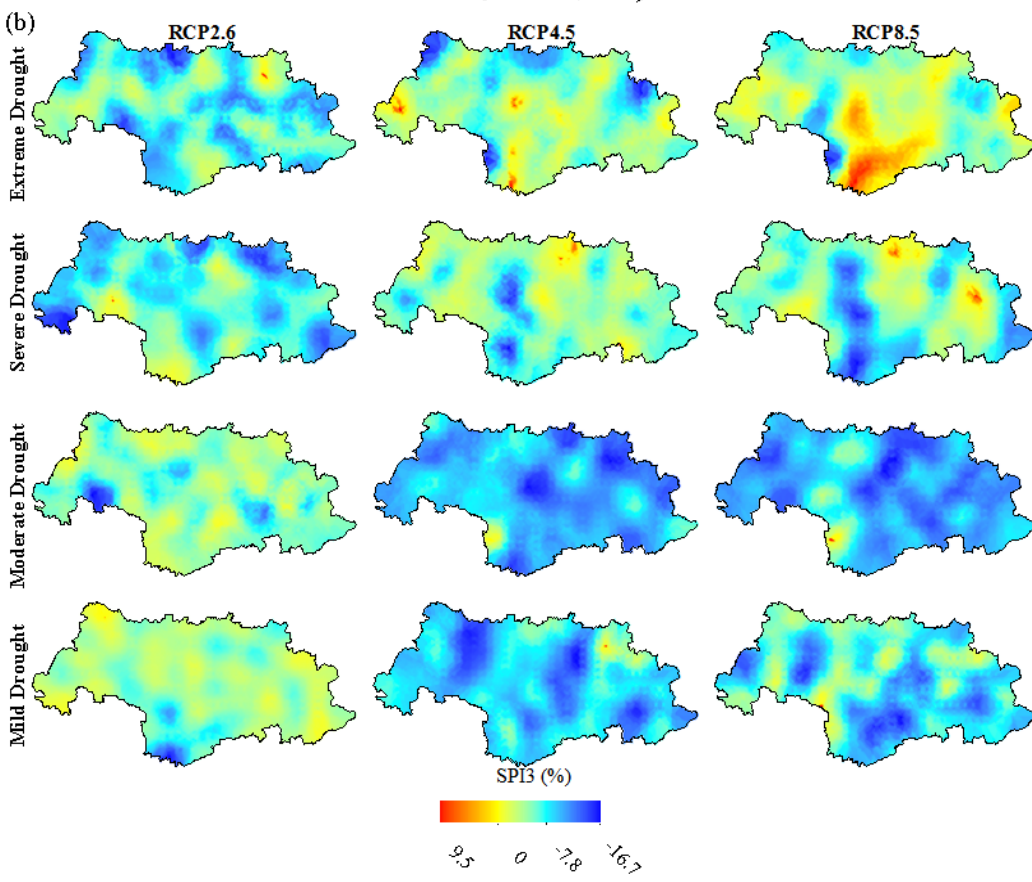


1052 **Fig.6.** Box plots of relative change (%) in D_F indicated by PDSI (≤ -1), SPI3 (≤ -0.5) and
 1053 SPEI3 (≤ -0.5) under 3 RCP (RCP2.6, RCP4.5 and RCP8.5) scenarios for the future
 1054 period 2021-2050 (relative to the baseline period 1971-2000) in the West River (a) and
 1055 North River (b) basins. Boxes indicate the interquartile model spread (25th and 75th
 1056 quantiles) with the red horizontal line indicating the ensemble median and the whiskers
 1057 showing the extreme range of the 30 simulation samples of the 13 CMIP5 GCMs. Black
 1058 circles denote the average of the multi-model ensembles.

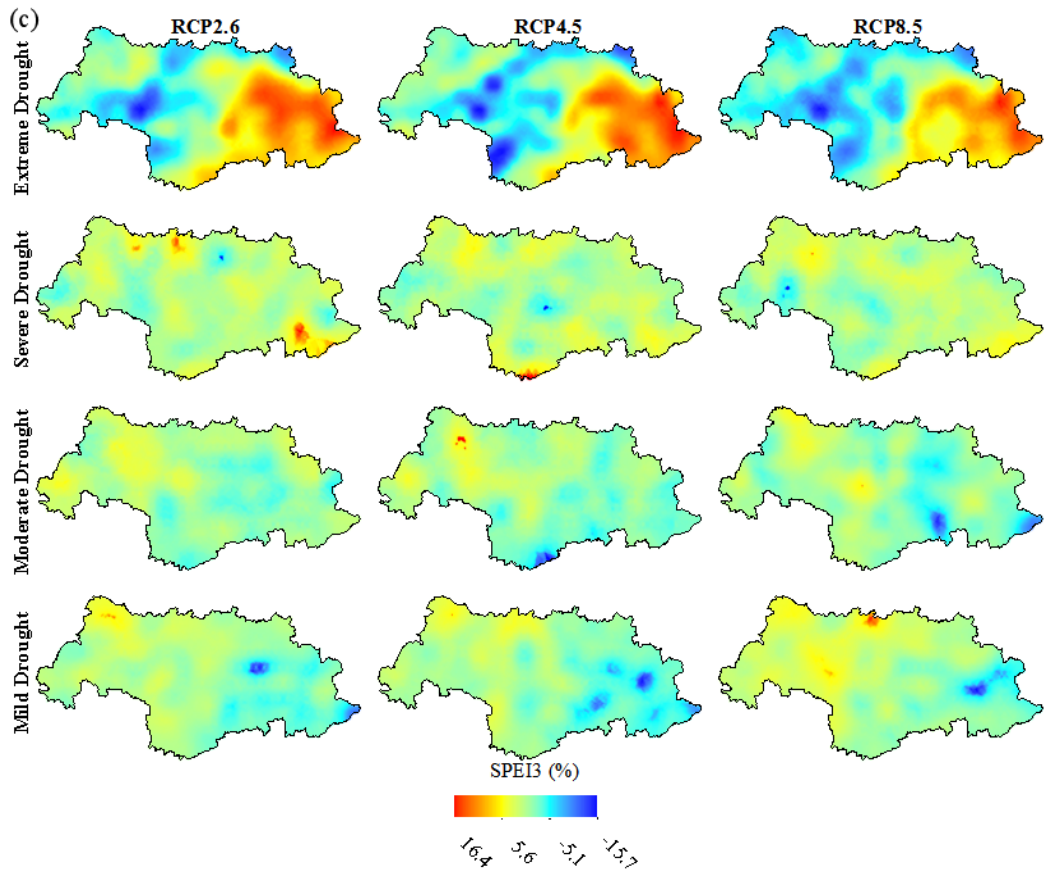
1059



1060

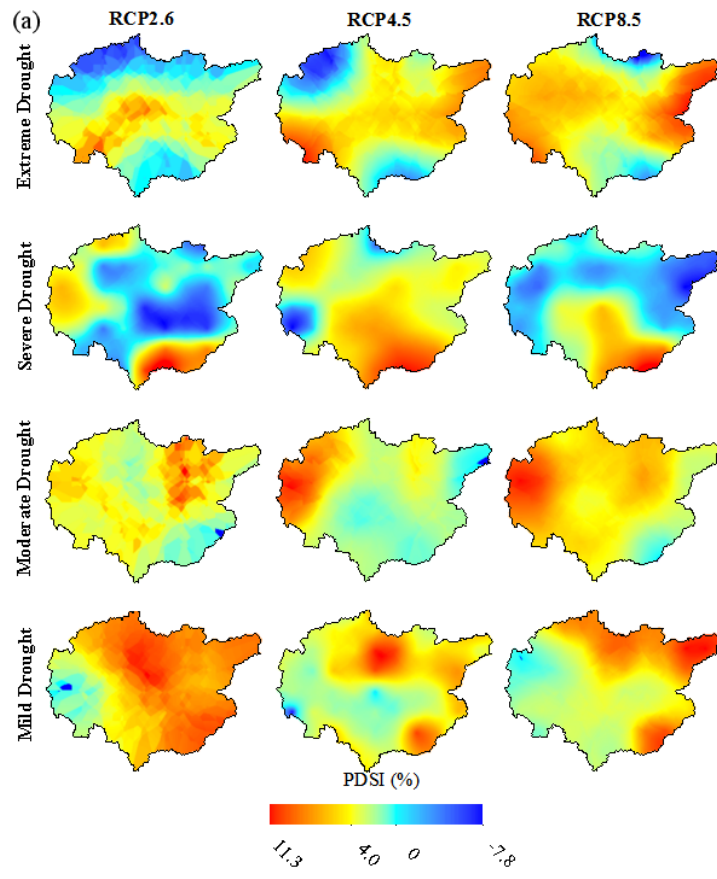


1061

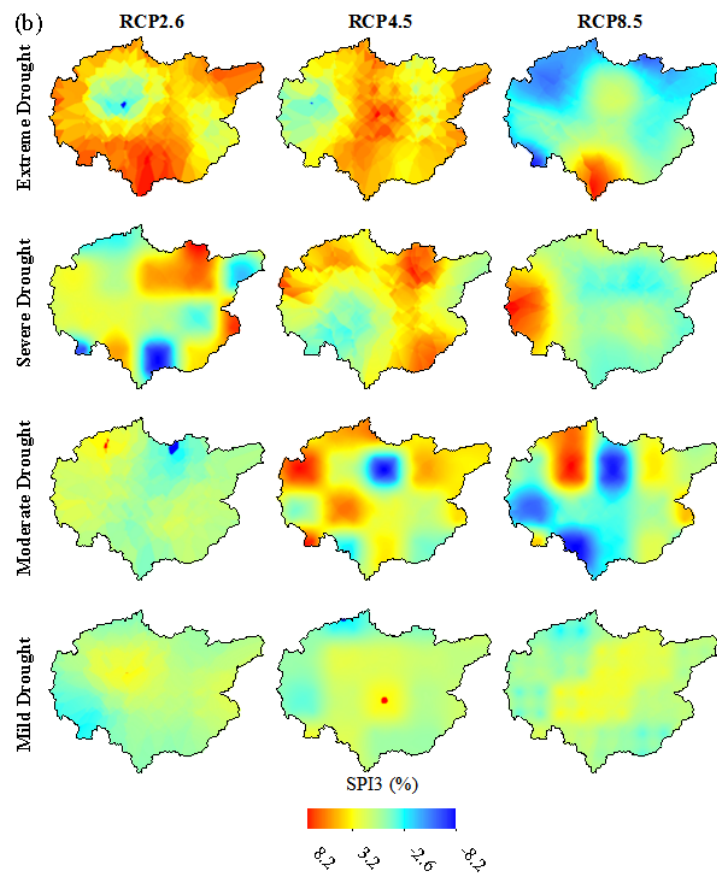


1062
 1063
 1064
 1065
 1066
 1067

Fig.7. Spatial distributions of D_F (%) indicated by PDSI (a), SPI3 (b) and SPEI3 (c) with extreme, severe, moderate and mild droughts in the future period 2021-2050 (relative to baseline period 1971-2000) under RCP2.6, RCP4.5 and RCP8.5 scenarios in the West River basin.



1068



1069

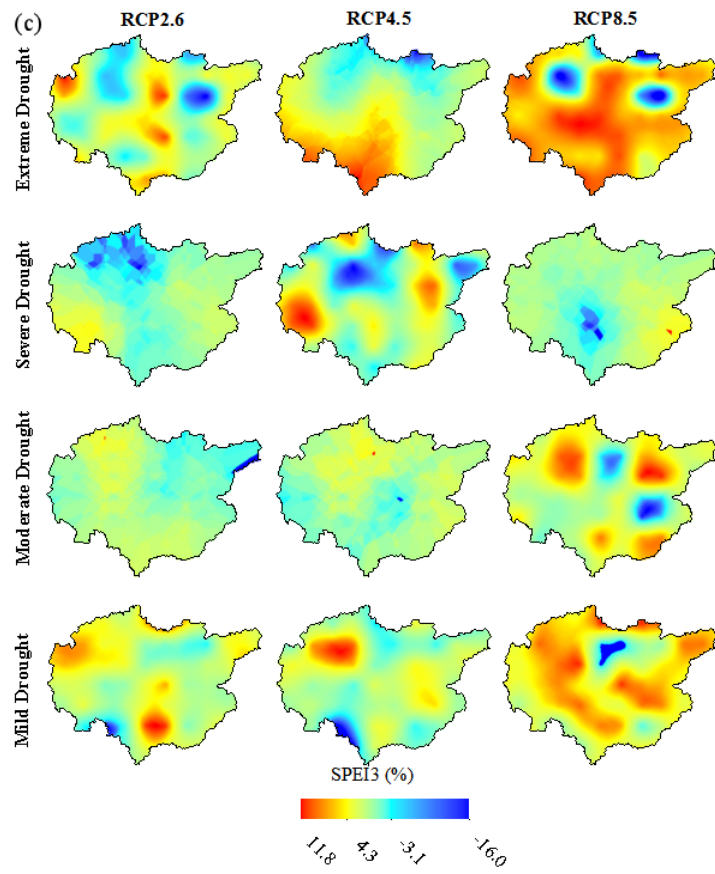
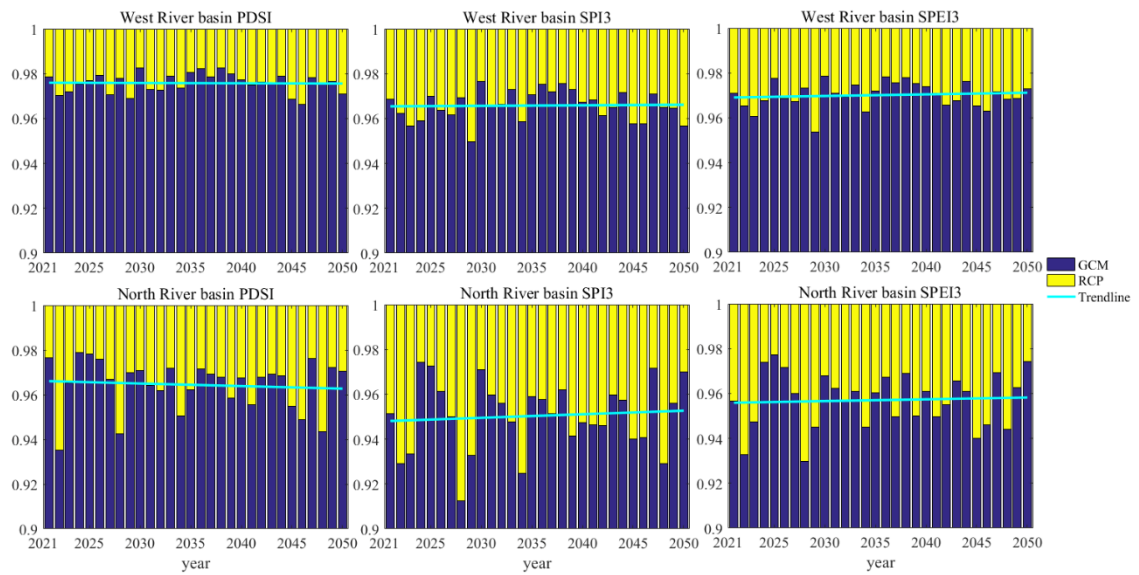


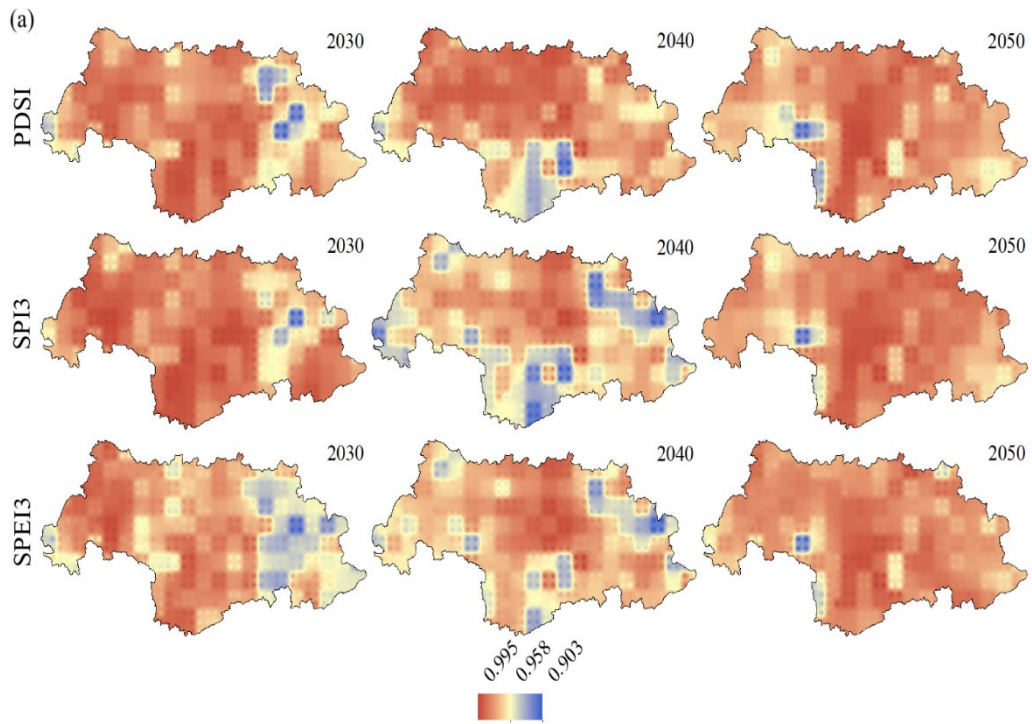
Fig.8. Same as Fig. 7 but for the North River basin.

1070
1071
1072

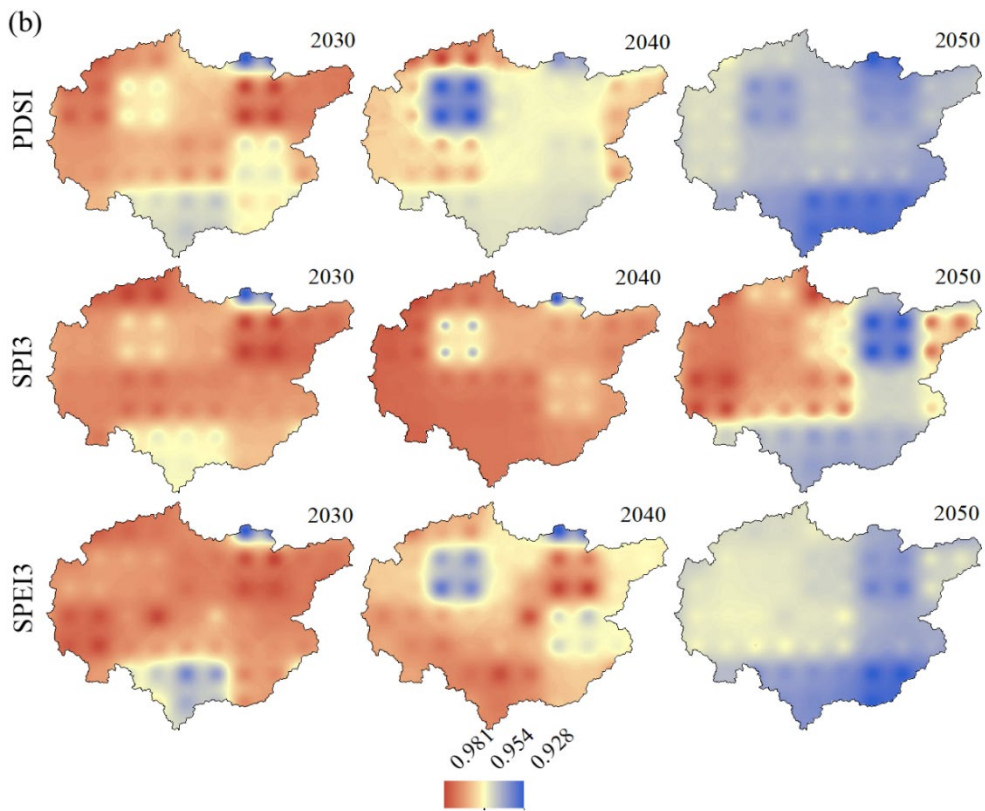


1073
 1074
 1075
 1076
 1077
 1078

Fig.9. Time series of relative contribution of GCM (blue) and RCP (yellow) to the projection uncertainty of PDSI, SPI3 and SPEI3 in the West and North River basins in the future period 2021-2050. The blue solid line indicates the linear trend of GCM uncertainty.



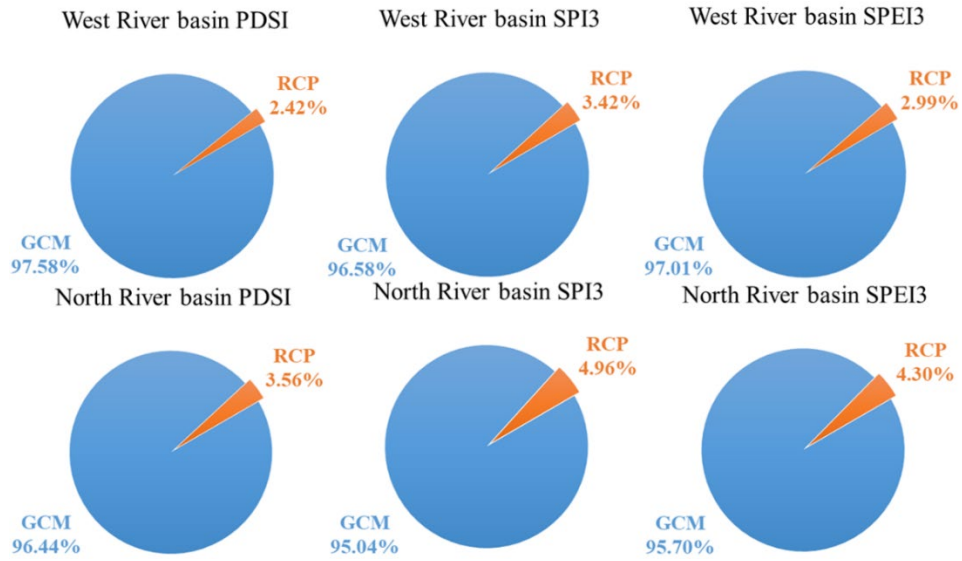
1079



1080

1081 **Fig.10.** Spatial distributions of the uncertainty contribution GCM to the projections of
 1082 PDSI, SPI3 and SPEI3 in the West River (a) and North River (b) basins in 2030, 2040
 1083 and 2050.

1084



1085

1086

1087

1088

Fig.11. Relative contribution rate (%) of GCM and RCP to the projection uncertainty of PDSI, SPI3 and SPEI3 in the West and North River basins.

1089 Table 1 Information on the 13 general circulation models used in the present analysis

Model	Institution	Country	Resolution
BCC-CSM1.1	Beijing Climate Center (BCC), China Meteorology Administration, China	China	128×64
BNU-ESM	Beijing Climate Center College of Global Change and Earth System Science, Beijing Normal University, China	China	128×64
CNRM-CM5	Centre National de Recherches Meteorologiques and Centre Europeen de Recherches et de Formation Avancee en Calcul Scientifique	France	256×128
GFDL-CM3	National Oceanic and Atmospheric Administration (NOAA) Geophysical Fluid Dynamics Laboratory	America	144×90
GFDL-ESM2G	National Oceanic and Atmospheric Administration (NOAA) Geophysical Fluid Dynamics Laboratory	America	144×90
GISS-E2-R	NASA Goddard Institute for Space Studies	America	144×90
HadGEM2-ES	Met Office Hadley Centre	United Kingdom	192×145
MIROC5	Atmosphere and Ocean Research Institute (The University of Tokyo), National Institute for Environment Studies, and Japan Agency for Marine-Earth Science and Technology	Japan	256×128
MIROC-ESM-CHEM	Japan Agency for Marine-Earth Science and Technology, Atmosphere and Ocean Research Institute (The University of Tokyo), and National Institute for Environment Studies	Japan	128×64
MIROC-ESM	Japan Agency for Marine-Earth Science and Technology, Atmosphere and Ocean Research Institute (The University of Tokyo), and National Institute for Environment Studies	Japan	128×64
MPI-ESM-LR	Max Planck Institute for Meteorology	Germany	192×96
MRI-CGCM3	Meteorological Research Institute	Japan	320×160
NorESM1-M	Norwegian Climate Centre	Norway	144×96

1090

1091

Table 2 Drought Classification based on PDSI, SPI and SPEI

Categories	PDSI classifications	SPI classifications	SPEI classifications
Extremely Drought (Ex_D)	$PDSI \leq -4.00$	$SPI \leq -2.0$	$SPEI \leq -2.0$
Severely Drought (Se_D)	$-3.99 \leq PDSI \leq -3.00$	$-1.99 \leq SPI \leq -1.5$	$-2.0 < SPEI \leq -1.5$
Moderately Drought (Mo_D)	$-2.99 \leq PDSI \leq -2.00$	$-1.49 \leq SPI \leq -1.0$	$-1.5 < SPEI \leq -1.0$
Mild Drought (Mi_D)	$-1.99 \leq PDSI \leq -1.00$	$-0.99 \leq SPI \leq -0.5$	$-1.0 < SPEI \leq -0.5$

1092

1093